Journal of Geophysical Research: Space Physics

REVIEW ARTICLE
10.1002/2017JA024203

**Key Points:**
- Interplanetary turbulence in high-speed streams is reviewed from a microstructual observational viewpoint for the first time
- Single wave characteristics can give information on the development of turbulence
- Single wave "period doubling" and "wave breaking" have been found

**Correspondence to:**
B. T. Tsurutani,
bruce.t.tsurutani@jpl.nasa.gov

**Citation:**
Tsurutani, B. T., Lakhina, G. S., Sen, A., Hellinger, P., Glassmeier, K.-H. & Mannucci, A. J. (2018). A review of Alfvénic turbulence in high-speed solar wind streams: Hints from cometary plasma turbulence. *Journal of Geophysical Research: Space Physics*, *123*. https://doi.org/10.1002/2017JA024203

Received 4 APR 2017
Accepted 4 NOV 2017
Accepted article online 6 FEB 2018



# A Review of Alfvénic Turbulence in High-Speed Solar Wind Streams: Hints From Cometary Plasma Turbulence

**Bruce T. Tsurutani[1], Gurbax S. Lakhina[2], Abhijit Sen[3], Petr Hellinger[4], Karl-Heinz Glassmeier[5], and Anthony J. Mannucci[1]**

[1]Jet Propulsion Laboratory, California Institute of Technology, Pasadena, CA, USA, [2]Indian Institute of Geomagnetism, Navi Mumbai, India, [3]Institute for Plasma Research, Gandhinagar, India, [4]Astronomical Institute, CAS, Prague, Czech Republic, [5]Technical University of Braunschweig, Braunschweig, Germany

**Abstract** Solar wind turbulence within high-speed streams is reviewed from the point of view of embedded single nonlinear Alfvén wave cycles, discontinuities, magnetic decreases (MDs), and shocks. For comparison and guidance, cometary plasma turbulence is also briefly reviewed. It is demonstrated that cometary nonlinear magnetosonic waves phase-steepen, with a right-hand circular polarized foreshortened front and an elongated, compressive trailing edge. The former part is a form of "wave breaking" and the latter that of "period doubling." Interplanetary nonlinear Alfvén waves, which are arc polarized, have a ~180° foreshortened front and with an elongated trailing edge. Alfvén waves have polarizations different from those of cometary magnetosonic waves, indicating that helicity is a durable feature of plasma turbulence. Interplanetary Alfvén waves are noted to be spherical waves, suggesting the possibility of additional local generation. They kinetically dissipate, forming MDs, indicating that the solar wind is partially "compressive" and static. The ~2 MeV protons can nonresonantly interact with MDs leading to rapid cross-field (~5.5% Bohm) diffusion. The possibility of local (~1 AU) generation of Alfvén waves may make it difficult to forecast High-Intensity, Long-Duration AE Activity and relativistic magnetospheric electrons with great accuracy. The future Solar Orbiter and Solar Probe Plus missions should be able to not only test these ideas but to also extend our knowledge of plasma turbulence evolution.

**Plain Language Summary** Interplanetary Alfvénic turbulence is studied from an observational microstructural viewpoint. We use cometary turbulence as a guide and for comparison to interplanetary turbulence. It is shown that single wave cycles reveal much of the ongoing physics. Alfvén waves phase-steepen forming a high-frequency end, leaving a low-frequency end. This is a form of "wave breaking" and "period doubling" occurring at the same time. If Alfvén waves occur at all scale sizes, this can explain the Kolmogrov-type spectra found in all studies. The interplanetary medium is also highly "compressive." This is caused by the magnetic decreases detected at the ends of the Alfvén waves. It is thought that this is a kinetic process associated with the dissipation of the Alfvén waves. The interplanetary Alfvén waves are often arc-polarized spherical waves implying a local source of generation. Some theoretical mechanisms for local generation are cited. Finally, it is shown that the MDs can cause rapid cross-field diffusion of energetic solar flare particles, perhaps explaining their broad distributions in solar longitude. Single cycle Alfvén waves impinging on the magnetosphere cause strong and continuous auroral activity.

## 1. Introduction

The solar wind at low heliospheric latitudes is composed of a broad range of spatial and temporal scales from discontinuities of seconds (with proton gyroradii scale lengths) to minutes duration (Belcher & Davis, 1971; Burlaga, 1971; Colburn & Sonett, 1966; Horbury & Tsurutani, 2001; Lepping & Behannon, 1986; Neugebauer, 2006; Neugebaueer & Giacalone, 2010; Smith, 1973a, 1973b; Tsurutani & Ho, 1999; Tsurutani & Smith, 1979; Vasquez et al., 2007) and Alfvén waves which range in scale from minutes to days and even weeks (Belcher & Davis, 1971; Matteini et al., 2015; Tsurutani, Gonzalez et al., 1995; Tsurutani et al., 2006; Tsurutani, Smith, et al., 1995). All of these waves and structures are contained within the supersonic solar wind. The structures are convected outward from the Sun at the solar wind speed. There are two basic types of solar wind. There is the slow solar wind with speeds of ~300 to 450 km $s^{-1}$. This wind comes from solar coronal streamers or their vicinity (Nerney & Suess, 2005; Suess & Nerney, 2002). The high-speed streams

(HSSs) have speeds of ~750 to 800 km $s^{-1}$ and come from solar coronal holes (Krieger et al., 1973; McComas et al., 2002; Neupert & Pizzo, 1974; Phillips et al., 1994; Tsurutani, Echer, & Gonzalez, 2011).

There are also transients which propagate into the interplanetary medium. Fast transients such as interplanetary coronal mass ejections (ICMEs) cause the formation of fast collisionless shocks (Echer et al., 2011; Gold, 1955; Kennel et al., 1985; Levy et al., 1964; Lugaz et al., 2016; Sonett & Abrams, 1963; Ness et al., 1964; Oliveira & Raeder, 2015; Papadopoulos, 1985; Tsurutani & Lin, 1985) ahead of the solar-origin plasma and field structures. These shocks cause heating and compression of the upstream (antisunward side) slow solar wind plasma, forming sheaths between the shocks and the ICMEs (Echer et al., 2008; Hundhausen, 1985; Tsurutani et al., 1988). At 1 AU these sheaths have a scale size of approximately hours. There is smaller scale, large-intensity turbulence within the sheaths (Tsurutani et al., 1988). The sizes of the magnetic cloud (MC) portions of the ICMEs are by definition >24 hr in duration (Burlaga et al., 1981; Klein & Burlaga, 1982) or approximately greater than 1 day in duration.

High-speed streams are also interplanetary transients. HSSs interact with upstream slow-speed streams forming interplanetary "corotating" interaction regions (CIRs; Smith & Wolfe, 1976; Tsurutani, Gonzalez, et al., 1995). CIRs are compressive regions of heated and accelerated slow-speed plasma and fields on the antisunward side and heated and decelerated HSS plasma and fields on the sunward side (Pizzo, 1985). The two sides of the CIR are separated by a tangential discontinuity. CIRs have scale sizes of ~10 to 20 hr (Tsurutani, Gonzalez, et al., 1995) at ~1 AU from the Sun. At ~1.5 AU from the Sun and beyond, CIRs are typically bounded by fast forward shocks (FSs) on the antisunward side and fast reverse shocks on the sunward side (Echer et al., 2010; Smith & Wolfe, 1976; Tsurutani, Smith, Pyle, et al., 1982).

Researchers of the interplanetary medium have suggested that the dynamical solar wind is prone to the development of a turbulent cascade. In particular, because broad portions of the magnetic fluctuation spectrum typically have power law structures close to $f^{-5/3}$, suggesting a Kolmogorov, hydrodynamic-like turbulence, it is thought that the turbulence will have an anisotropic orientation due to the presence of a strong magnetic guide field (Bruno & Carbone, 2013; Matthaeus & Velli, 2011; Montgomery & Turner, 1981; Shebalin et al., 1983; Verdini & Grappin, 2016).

The solar wind is considerably simpler at high heliospheric latitudes. During the descending phase of the solar cycle, the polar regions of the Sun are dominated by large coronal holes. Thus, there is only the high-speed solar wind present at these high latitudes. This high-speed wind will not have upstream slow solar winds to interact with, so there will not be any CIRs formed (Tsurutani et al., 2009). Solar ARs are confined to latitudes less than ~35°, so there are few ICME transients at these high latitudes, if any. On the other hand, the solar wind is characterized by large-amplitude Alfvénic waves (Belcher & Davis, 1971; Tsurutani, Smith, et al., 1995; Tsurutani, Gonzalez et al., 1995; Tsurutani et al., 1996), and the main portion of the magnetic field power spectrum is characterized by a Kolmogorov-like spectrum.

Our effort in this review will be to examine the turbulence in the HSSs at high heliospheric latitudes. We will present a short review of cometary plasma turbulence to give the reader an idea on how much information about turbulence can be gained from examining magnetic fields and plasma microstructures. Thus, for the study of interplanetary turbulence, an emphasis will be made on the Ulysses magnetic field and plasma microstructure such as discontinuities, shocks, and magnetic decreases (MDs). Individual Alfvén wave evolution will be examined in detail. It is felt that understanding the high-latitude solar wind turbulence will help us understand the more complex near-equatorial turbulence. Even though dynamical cases such as ICMEs and CIRs will not be present, it will be shown that the evolution of turbulence is still occurring. Using these fast solar wind observations of "Alfvénic" turbulence, arguments will be made for a different type of cascade process than normally assumed. It is clear that these ideas will be relevant for equatorial interplanetary turbulence as well. This can be easily tested using interplanetary spacecraft data. Some of the obvious predictions can be tested using the upcoming Solar Orbiter (Marsch et al., 2005) (http://sci.esa.int/solar-orbiter/) and Solar Probe Plus (Fox et al., 2015) (http://solarprobe.jhuapl.edu/The-Mission/index.php) plasma, field, and energetic particle data. In this paper, we will indicate scientific topics ripe for examination of plasma phenomena made closer to the Sun.

There have been many reviews of interplanetary turbulence written with emphasis on a magnetohydrodynamic (MHD) approach. There have also been a few reviews written on the topic of discontinuities, shocks, and MDs. However, to our knowledge, there has never been a review with the emphasis on how discontinuities, shocks, MDs, and Alfvén wave evolution may play a role in interplanetary turbulence. This is the goal of

the present paper. In section 2.1, we will show the interplanetary magnetic power spectra and briefly discuss their possible implications. Section 2.2 will address cometary magnetic turbulence examples to show that other means of diagnostics besides power spectra are important as well. In particular, it will be emphasized that examination of single wave cycles to determine waveforms and helicity provide much needed information on the development and nature of a specific type of plasma turbulence. Section 2.3 introduces observations of Alfvén waves and MDs present in HSSs. Sections 2.4–2.7 introduce and discuss discontinuities and shocks and previous work on these phenomena. Their contributions to interplanetary turbulence are emphasized. Section 2.7 examines single cycle Alfvén waves in a manner similar to the examination of single cycle cometary waves. Although previous publications have discussed such observational features, new insights in terms of turbulence development emerge. Section 2.8 shows the relationship between Alfvén waves and MDs and discusses in detail theories and models of MD development. MDs are the main "compressional" component of interplanetary turbulence, and theories which do not contain an explanation of these features are not complete. Section 3 is a brief summary of all of the subsections of section 2. This section is an attempt to bring all of the interplanetary microstructure features and their evolution together as a whole. Section 4 discusses some of the observations of the Alfvén waves of section 2.7 with the possibility of local generation. Section 5 discusses the consequences of the interplanetary microstructure. In particular, section 5.1 briefly reviews the effects of MDs on cross-field diffusion of solar energetic particles, and section 5.1 reviews new revelations of individual Alfvén wave cycles on geomagnetic activity at Earth and the production of relativistic magnetospheric electrons. A final set of comments on current problems are given in section 6.

## 2. Results

### 2.1. Interplanetary Power Spectra

Typical power spectra of the interplanetary magnetic field taken over 2 day intervals are shown in Figure 1. On the left are the transverse and field magnitude power spectra taken at −1.9° heliospheric latitude ~1.8 AU from the Sun. On the right are the same parameters taken at −79° heliospheric latitude ~2.4 AU from the Sun. The intervals were chosen such that the radial distances from the Sun were comparable. The high-latitude data were taken while the Ulysses spacecraft was in an HSS associated with a polar coronal hole. The frequencies displayed for all four spectra extend from almost ~$10^{-5}$ to ~$10^{-1}$ Hz.

What is remarkable is that all four spectra in Figure 1 have approximately the same power law forms. Linear curve fits in the log-log plots were made to all four spectra, and the results are displayed in each panel. Each of the spectra has an $f^{-1.5}$ to $f^{-1.7}$ power law dependence, consistent with the idea that the turbulence both in the ecliptic plane and in HSSs are Kolmogorov in nature.

It should be noted that the interplanetary medium is "compressive," that is, that there is substantial power in the spectra of the magnetic field magnitude. This is an important point and will be addressed later in this paper.

The transverse wave power over the poles is a factor of ~2 times larger than in the ecliptic ($2.0 \times 10^{-4}\, f^{-1.7}$ compared with $1.0 \times 10^{-4}\, f^{-1.6}$). The same is true for the magnetic magnitude power. The spectra are ~2 times larger at high latitudes. Further details are given in Tsurutani and Ho (1999). These points will be revisited later.

It should be mentioned that other published interplanetary power spectra (Horbury & Tsurutani, 2001) have shown an ~$f^{-1}$-dependent component at the lowest part of the spectrum (between ~$10^{-4}$ and $10^{-5}$ Hz). The spectra in Figure 1 do not cover those frequencies well. However, this is not particularly important for our discussion here.

### 2.2. Cometary Plasma Turbulence

We deviate for a moment to briefly discuss cometary plasma waves and turbulence. After the nature of cometary turbulence is explained, we will show how similar analysis techniques will lead an interpretation of interplanetary turbulence. In later sections, we will apply the same techniques to interplanetary Alfvén waves. Figure 2 gives a schematic which shows why there are intense plasma waves around a comet.

Figure 2 shows a schematic of cometary ion pickup in the solar wind. The comet nucleus is on the right, and the Sun is on the left (not shown). The solar wind is flowing from left to right at speeds of ~400 km/s (here we assume the slow solar wind). As the comet approaches the Sun, the volatiles in the nucleus sublimate from its

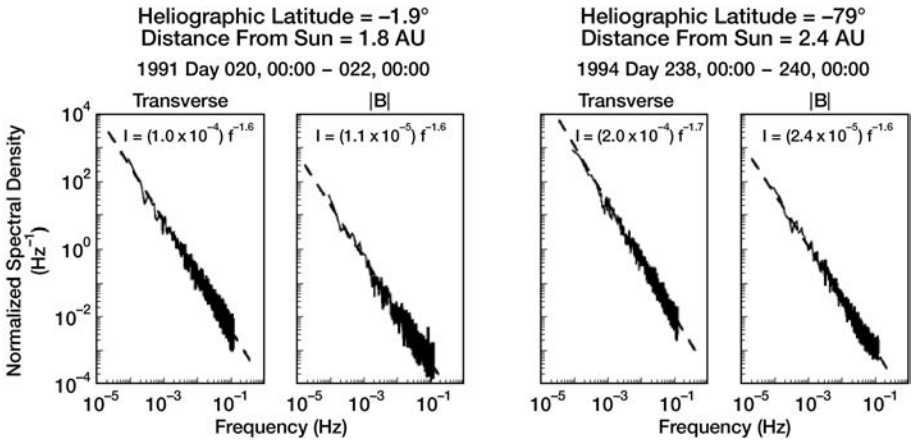


**Figure 1.** Examples of the interplanetary magnetic field power spectra from the Ulysses spacecraft magnetometer. The two panels on the left are the transverse component and magnetic field magnitude power spectra for the solar wind in the ecliptic plane. The two panels on the right were taken at high heliospheric latitudes. The spectra extend from almost ~$10^{-5}$ to ~$10^{-1}$ Hz. Adapted from Tsurutani and Ho (1999).

surface and the molecules propagate at speeds of ~1 km/s radially away from the comet. The volatile material is mostly water-ice. It takes ~$10^6$ s for the molecules/atoms to get ionized by either photoionization or solar wind plasma charge exchange. When this occurs, the newly formed $H_2O$ group of ions ($H_2O^+$, $OH^+$, and $O^+$) experience the Lorentz force associated with the magnetic fields embedded in the flowing solar wind and become ions gyrating in the solar wind with speeds of ~400 km $s^{-1}$ (whatever the solar wind speed is). This pickup process forms an ion "ring," which is unstable to a $T\perp/T_{||} > 1$ instability. In the above $T\perp$ is the temperature perpendicular to the ambient magnetic field, and $T_{||}$ is the temperature parallel to the ambient magnetic field. The result is the generation of ion cyclotron (left-hand) waves. The freshly created ion plasma waves can then evolve and cascade. This solar wind magnetic configuration occurred at comet Grigg-Skjellerup, and the generation of nonlinear left-hand ion cyclotron waves has been well documented (Glassmeier & Neubauer, 1993).

What if the interplanetary magnetic field were parallel to the solar wind velocity instead of being perpendicular? Then the freshly created ions would not experience a Lorentz force. However, the ions would constitute a beam propagating with a speed of ~400 km $s^{-1}$ in the reference frame of the solar wind plasma and would therefore be subjected to a $T_{||}/T\perp \gg 1$ instability. This anisotropy will lead to the generation of right-hand (RH) polarized waves. This was the case for comet Giacobini-Zinner, the first observation of cometary waves and turbulence (Tsurutani & Smith, 1986a, 1986b). For more details about the instabilities and wave generation, we refer the reader to the seminal paper by Wu and Davidson (1972). A good review of the ion pickup process and the different wave modes that can be generated can be found in Tsurutani (1991).

Since the $H_2O$ neutral molecules can propagate at speeds of ~1 km $s^{-1}$ for ~$10^6$ s before they are ionized, the cometary turbulence can extend to ~$10^6$ km and further from the nucleus (Tsurutani, Brinca, et al., 1989; Tsurutani, Page, et al., 1989). Thus, cometary turbulence exists over an enormous volume around an active comet (one in close proximity to the Sun).

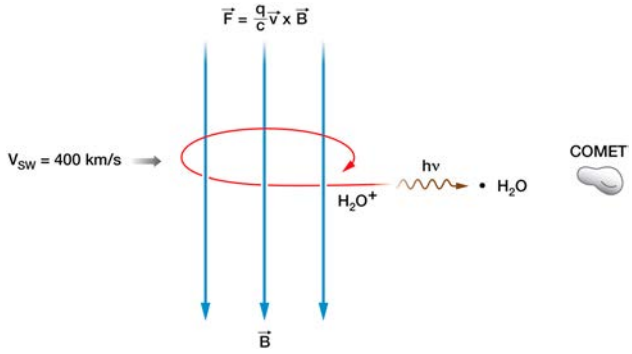


**Figure 2.** Pickup of a cometary ion in the solar wind. In the above schematic, the interplanetary magnetic field carried by the solar wind is orthogonal to the direction of solar wind flow.

In Figure 2, the spacecraft speed Vsc relative to the cometary nucleus is low (Vsc ~0 to 60 km $s^{-1}$) compared to the solar wind speed Vsw. Thus, the spacecraft instrumentation will view the plasma waves and turbulence essentially in the comet frame. The spacecraft sensors detect the plasma wave frequency and polarization in the cometary ion frame. In this case this will be at the $H_20$ group ion cyclotron frequency.

The three panels of Figure 3 show the transverse magnetic field power spectra of the turbulence at three different comets. The pickup ion cyclotron frequency "pump" wave is noted at

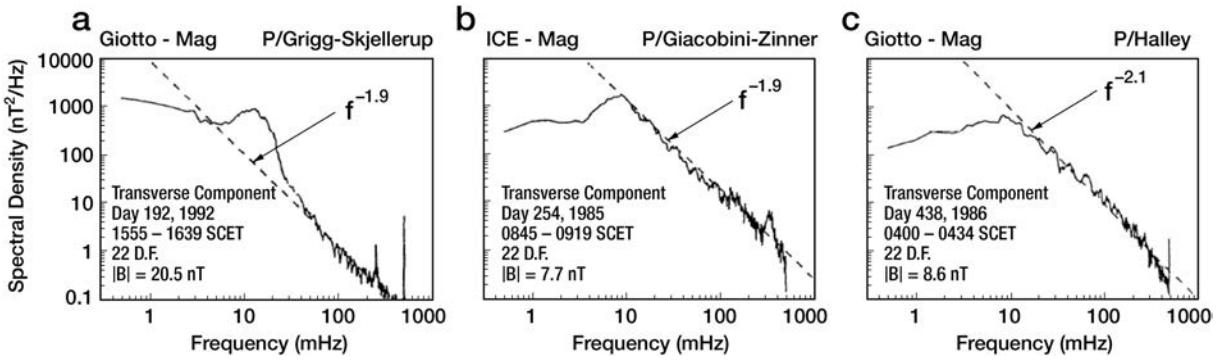


**Figure 3.** Power spectra of the transverse component of magnetic turbulence at three different comets: (left) Grigg-Skjellerup, (middle) Giacobini-Zinner, and (right) Halley. All three clearly display the $H_20$ group ion cyclotron frequency "pump wave" at ~10 mHz. The turbulence at frequencies higher than the pump frequency is fitted by power laws (dashed lines). The figure is adapted from Tsurutani, Glassmeier, and Neubauer (1995).

~10 mHz. All three power spectra display a power law spectrum at frequencies above the pump frequency. The power law fits range from $f^{-1.9}$ to $f^{-2.1}$. All three spectra have power laws close to $f^{-2.0}$. Thus, one might suspect that this is associated with Kraichnan turbulence (Kraichnan, 1965).

However, there is more information to be gained from the magnetic field data than simply spectral exponents. Information such as turbulence helicity (wave polarization) and waveforms are present and available. We thus next look at samples of the waveforms in Figure 4. As previously mentioned, there is a great deal of information available in single wave cycles.

Figure 4 displays the waveforms for the three comets shown in Figure 3. Even though the spectral shapes were similar, the waveforms are significantly different from each other. The waves at comet Grigg-Skjellerup (left-hand panel) are left-hand polarized waves (not shown) with periods of ~100 s. The peak-to-peak amplitudes in a ~24 nT magnetic field are ~20 nT. The magnetic field is compressive. However, what is important for the present discussion is that the waves are not sinusoidal. They are what we call "phase-steepened," meaning that there is more wave phase rotation on one side of the wave cycle than the other (see details in Tsurutani, Glassmeier, et al., 1995). It is this phase-steepening that is creating the high-frequency power in the spectrum of Grigg-Skjellerup in Figure 3. This phase-steepening plus some off-axis wave propagation is creating high-frequency power in the magnetic field magnitude spectrum as well (not shown).

The waves at comet Giacobini-Zinner (Figure 4, central panel) are RH polarized in the plasma frame (Brinca, 1991; Thorne & Tsurutani, 1987; Tsurutani & Smith, 1986a, 1986b; Tsurutani et al., 1987). These waves have

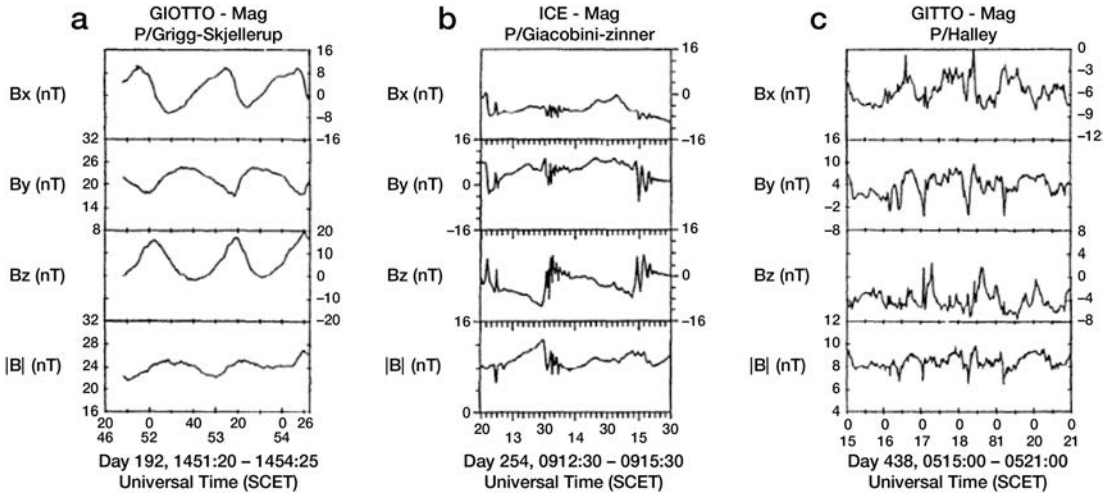


**Figure 4.** Sample waveforms of magnetic turbulence/waves at comets: (left) Grigg-Skjellerup, (middle) Giacobini-Zinner, and (right) Halley. The figure is an adaptation of Tsurutani, Glassmeier, and Neubauer (1995).

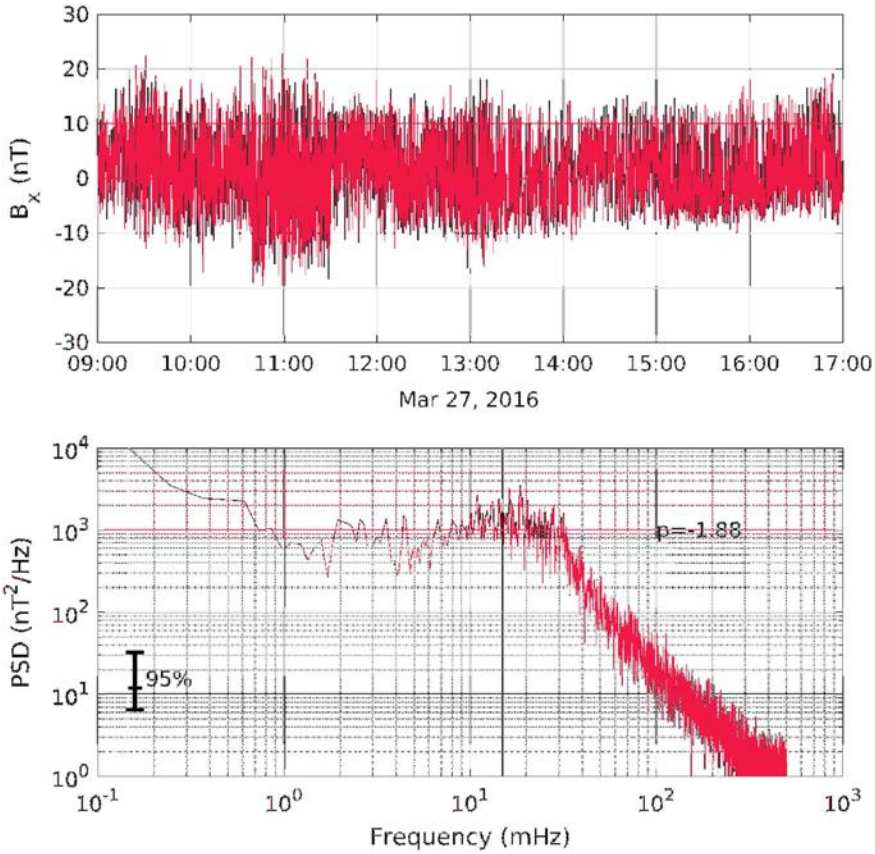


**Figure 5.** (top) Comet Churyumov-Gerasimenko "singing comet" waves and (bottom) power spectra. We note that these waves have a power spectrum of $\sim f^{-1.9}$ from $2 \times 10^1$ to $5 \times 10^2$ mHz. Adapted from Glassmeier (2017).

periods of ~100 s and have peak-to-peak component amplitudes of ~16 nT in an ~10 nT magnetic field. There are strong magnetic magnitude compressions of ~50%. The waves are phase-steepened and have a waveform considerably different than that of the left-hand Grigg-Skjellerup waves. There are large-amplitude high-frequency components which are not uniformly distributed throughout the interval but are primarily detected at the phase-steepened edges. These high-frequency components are part of the magnetosonic wave evolving toward "wave breaking." We refer the reader to Tsurutani, Brinca, et al. (1989) for further discussion of RH wave steepening and dispersion.

The RH panel of Figure 4 shows the waves at comet Halley. These waves have a mixture of polarizations (Glassmeier et al., 1987; Neubauer et al., 1986; Tsurutani et al., 1996) and may possibly be in a fully turbulent state. Since this is not the main thrust of this paper, we will not discuss this topic further.

Tsurutani, Glassmeier, et al. (1995) also showed the wave helicity differences for the three comets. These are also significantly different from one case to the next but have not been shown to conserve space. We refer the reader to the original article for further information and analysis techniques. Glassmeier et al. (1989) have studied this topic in detail.

We show two more examples of cometary waves and wave power spectra taken from the recent European Space Agency/NASA Rosetta spacecraft encounter with comet Churyumov-Gerasimenko (comet "C.-G."). Figure 5 (top) shows the large-amplitude (~20 nT peak-to-peak in an ~40 nT magnetic field) "singing comet" waves (Richter et al., 2015, 2016) which are not generated by ion pickup but presumably by a cross-current (modified ion Weibel) instability (Glassmeier, 2017). Although the waves appear to be a discrete mode, there is also a high-frequency wave portion above the pump frequency. What is of importance here is the high-frequency power which occurs from $2 \times 10^1$ to $5 \times 10^2$ mHz. The power law spectral shape is $\sim f^{-1.9}$, similar to the previously displayed cometary high-frequency power spectra.

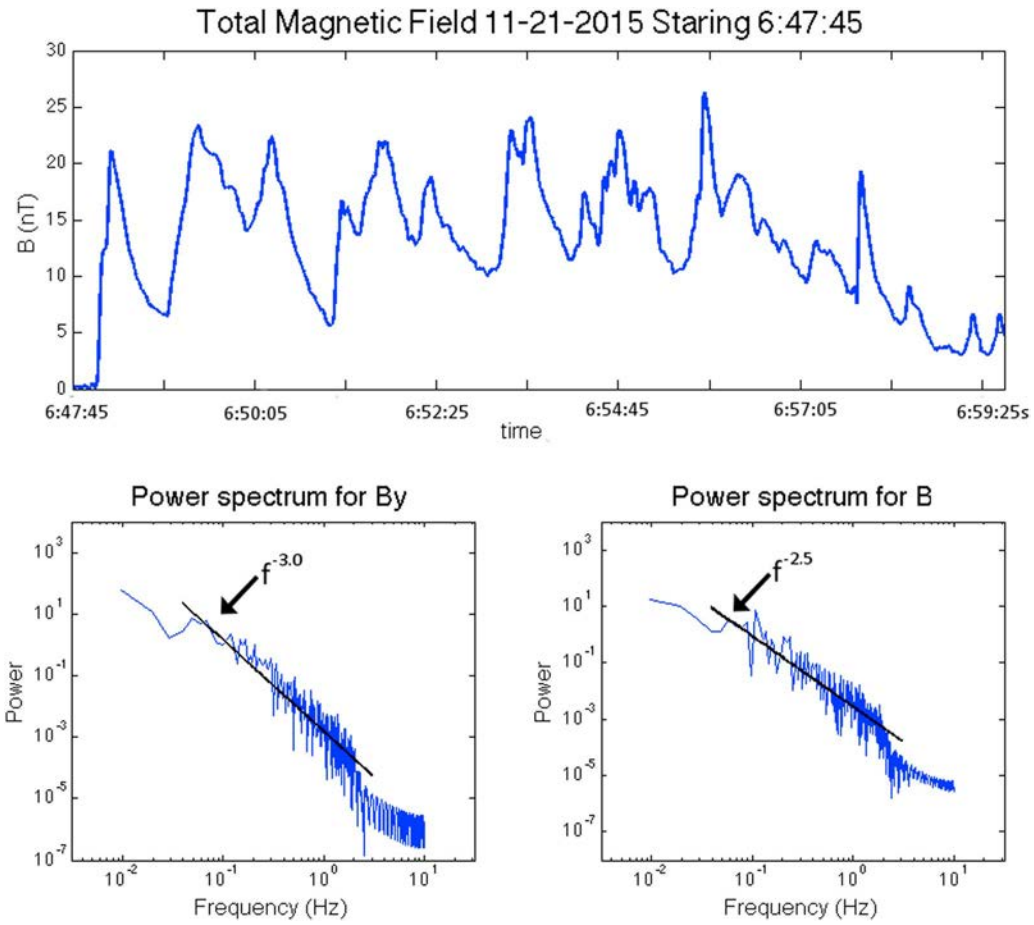


**Figure 6.** (top) Magnetic waveforms and (bottom) the power spectrum for the (left) By component of the waves and the (right) B field magnitude at comet C.-G.

A second example of nonlinear waves at comet C.-G. is shown in Figure 6. These waves were detected close to the comet diamagnetic cavity (Goetz, Koenders, Hansen, et al., 2016; Goetz, Koenders, Richter, et al., 2016). The individual wave cycles are asymmetric and have steepened edges on the left-hand side. A full analysis of the nature of these waves has not been completed yet, but it has been speculated that they are shocks (Tsurutani et al., 2016). The panel on the bottom left shows that the By field component has an ~$f^{-3.0}$ power law dependence from ~$4 \times 10^{-1}$ to 2 Hz and the $B$ field magnitude an ~$f^{-2.5}$ dependence over the same frequency range. So not all cometary power spectra have ~$f^{-2.0}$ spectra above the pump frequencies.

Figure 7 returns to the topic of magnetosonic wave steepening detected at comet Giacobini-Zinner. This example and information gained from it will be used as a guide to study single cycle Alfvén waves later in the paper. In the top panel slightly more than one wave cycle is shown. The compressional components of two wave peaks can be noted in the $B$ magnitude panel at ~717:40 and ~719:10 UT. The magnetic field magnitude increases by ~30 to 50%. At approximately the same time as these compressions, fluctuations in the $B_R$, $B_T$, and $B_N$ components are noted. These are associated with the phase-steepening of the magnetosonic waves. In the radial-tangential-normal (RTN) system, **R** points radially away from the Sun, **T** is $\boldsymbol{\Omega} \times \mathbf{R}/|\boldsymbol{\Omega} \times \mathbf{R}|$, where $\boldsymbol{\Omega}$ is the rotation axis of the Sun and **N** completes the RH coordinate system.

To better understand the phase-steepening process of these magnetosonic waves, a minimum variance analysis (Smith & Tsurutani, 1976; Sonnerup & Cahill, 1967) has been performed on a portion of the above interval which includes only one wave cycle. The minimum variance coordinates are determined by diagonalizing the covariance matrix of the three magnetic field components. The three eigenvectors represent the three principal directions, and the magnetic field is rotated into this system to obtain the B1, B2, and B3 components where B1 is the maximum variation component, B2 is the intermediate variance component, and B3 is the minimum variance component.

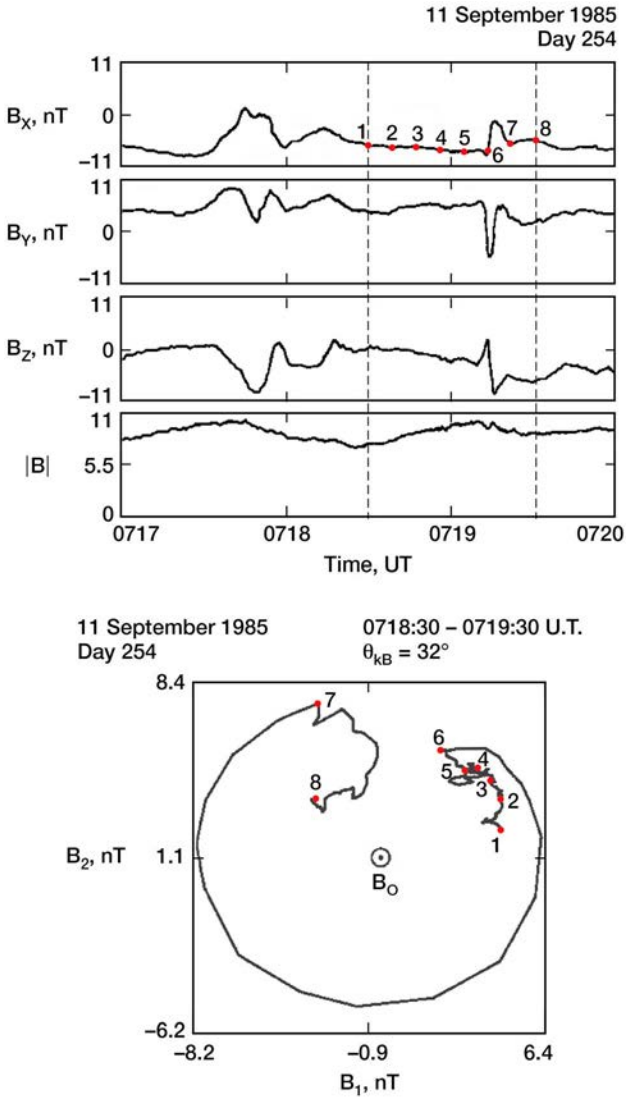


**Figure 7.** A phase-steepened magnetosonic wave detected at comet Giacobini-Zinner. (top) Three components of the wave in interplanetary radial-tangential-normal coordinates and the field magnitude. (bottom) Hodogram of the minimum variance B1 and B2 components of the magnetic field.

A hodogram of the B1 (maximum variance) versus the B2 (intermediate variance) component is shown in the bottom panel of the figure. The time interval of analysis is 0718:30 to 0719:30 UT. Corresponding time marks are indicated in the top and bottom panels so that the reader can follow the detailed spatial features of this wave.

Point 1 (beginning of the interval) starts where the magnetic field magnitude is a local minimum. The following points 2, 3, 4, 5, and 6 occur on the rising compressional part of the wave (top panel), with little or no wave phase rotation. This portion of the wave is linearly polarized and compressional. From points 6 to 7, almost all of the wave rotation occurs. This time interval is from ~0718:37 to ~0718: 50 UT (see top panel), an interval of only ~13 s. From the bottom panel it is clearly seen that the wave is circularly polarized. In the hodogram the ambient magnetic field direction is out of the paper, so the wave is left-hand polarized in the spacecraft frame. Since the wave is being convected by the solar wind past the spacecraft, it is anomalously Doppler-shifted, and thus, the wave is RH polarized in the plasma frame. The RH polarization and compressive nature of the wave indicate that it is propagating in the magnetosonic mode. This is in agreement with theory.

What one notes from this wave example is that the nonlinear phase-steepening process has moved all the RH rotation/helicity of the wave into a small region of space, ~13 s in duration (compared to the wave period of ~100 s). This steepening process has thus created a high-frequency component to the turbulence. An analogy to this is when an ocean wave approaches shore, the wave steepens more and more until it finally "breaks," creating high-frequency white foam on its leading edge. The steepening process of this magnetosonic wave is clearly creating high-frequency components before breaking. For magnetosonic waves, if the steepening process continues beyond the development of this particular example, they presumably develop into full scale fast mode shocks.

The other linearly polarized compressive part of the wave is also part of the cometary turbulence. This portion of the wave now has a longer wavelength, since the wave period of ~100 s has remained constant in this steepening process. So this is a linear compressive component of the cometary turbulence. This portion of the wave has a "period doubling" characteristic. A comparison between single cycle magnetosonic waves and single cycle Alfvén waves will be made later in the paper.

The technique of using raw interplanetary magnetic field and plasma data of single wave cycles will be employed to better understand interplanetary turbulence in high-speed solar wind streams in the next section. This information will be useful for improving our understanding of the development of turbulence at high heliospheric latitudes.

### 2.3. High-Latitude Solar Wind Turbulence: Alfvén Waves

Ulysses was launched in 1990 and then traveled to Jupiter, located at a distance ~5 AU from the Sun. The close swing-by with the planet gave Ulysses a gravitational assist to get it into an orbit which took it over the solar poles. It reached ~±80°. The trajectory to Jupiter and the first polar orbit are shown in Figure 8.

The solar wind velocity and magnetic field polarity for the first polar pass are shown in Figure 9. The speed of the solar wind at any point is indicated by the radius from the center of the Sun (in the figure) to the curve. The superposed image of the Sun was taken by the Solar and Heliospheric Extreme Ultraviolet Imaging Telescope soft X-ray detector (Delaboudinière et al., 1995). Polar coronal holes (dark regions) are noted in both the north

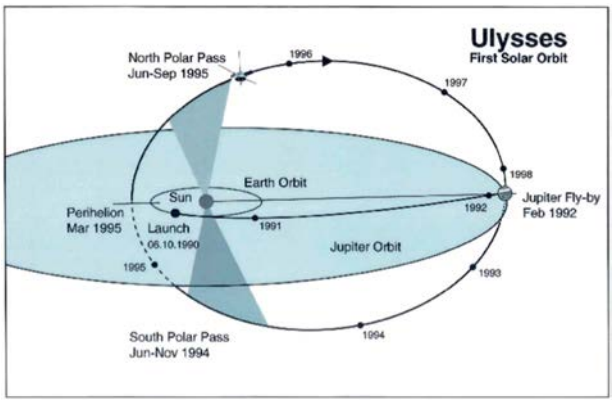


**Figure 8.** The orbit of Ulysses over the solar poles.

and south polar regions. The two coronagraph images identify helmet streamers near the equatorial plane. Ulysses traveled over the south pole from June to November 1994, during the declining phase of the solar cycle. Polar coronal holes are largest in extent during this phase of the solar cycle.

The magnetic field polarity is indicated by the coloration of the data plot. The northern hemisphere data are red, indicating outward pointing magnetic fields. The southern hemisphere data are blue, indicating inward pointing magnetic fields. During this phase of the solar cycle the solar magnetic field has a dipolar configuration (Jones & Balogh, 2003; Forsyth et al., 1996). Every ~11 years the polar magnetic fields reverse direction.

Figure 9 shows that the HSS coming out of the south polar coronal hole has speeds of ~750 to 800 km $s^{-1}$. This stream is long-lasting, and thus, there are no stream-stream interactions taking place between the Sun and the distance of Ulysses, ~2.2 AU away. By examining the solar wind turbulence in detail, the evolution leading to the power law spectra shown in Figure 1 will be better understood.

Figure 10 shows the magnetic field and solar wind velocity components within the polar HSS. From top to bottom are the solar wind $V_R$ and $B_R$ components, the $V_T$ and $B_T$ components, the $V_N$ and $B_N$ components, and the solar wind speed and magnetic field magnitude. The bottom panel indicates the spacecraft heliospheric latitude. The data are shown in the RTN coordinate system, described previously.

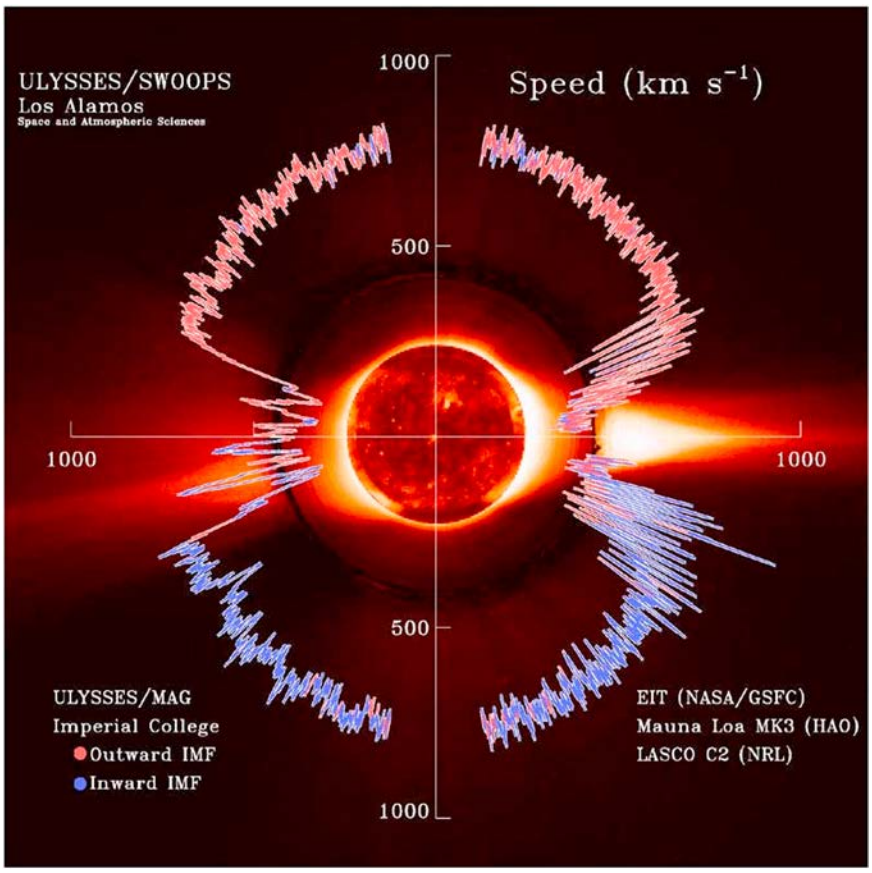


**Figure 9.** The solar wind speed and magnetic field polarity for the first Ulysses polar pass. There are gaps at ±80° to 90° because the spacecraft did not cover the heliospheric latitudes exactly at the poles. Taken from Phillips et al. (1994) and McComas et al. (2002).

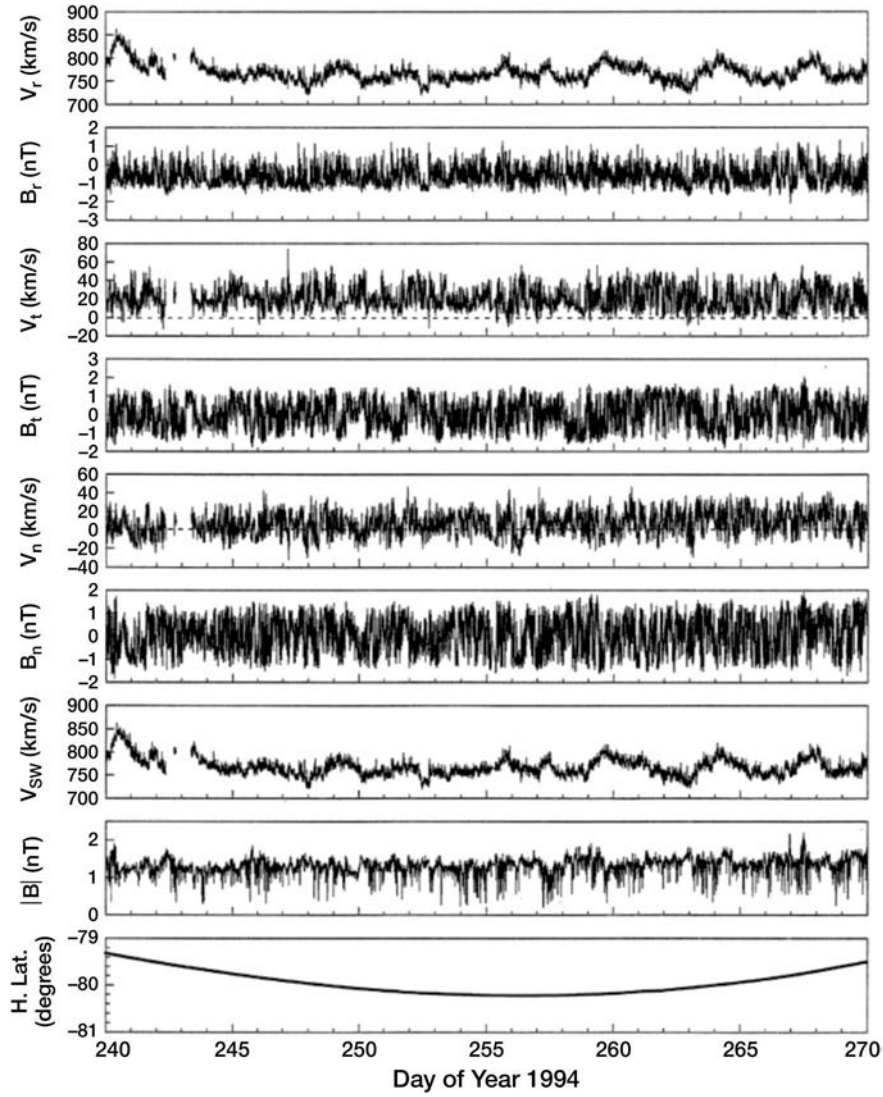


**Figure 10.** The magnetic field and solar wind velocity components over the south solar pole in radial-tangential-normal coordinates. The plot shows a 30 day interval when Ulysses was at heliospheric latitudes less than −79°. The figure is taken from Tsurutani, Lakhina, et al. (2005).

If one inspects the second, fourth, and sixth panels from the top, it can be noticed that the magnetic field components all vary between ~+1.0 and ~−1.0 nT. The eighth panel shows that the magnetic field magnitude $B_0$ is ~1.0 nT. These ever-present magnetic (and electric) oscillations have $\Delta\mathbf{B}/B_0$ ~1 to 2 and thus are highly nonlinear.

A second feature that is important for our discussion is the dips in the magnetic field magnitude (second panel from the bottom). The magnetic dips are ever-present and can be as large as 90% of the average ambient magnetic field strength. These are called MDs (Fränz et al., 2000; Neugebaueer & Giacalone, 2010; Stevens & Kasper, 2007; Tsubouchi, 2009; Tsubouchi & Matsumoto, 2005; Tsurutani, Lakhina, Verkhoglyadova, Echer, et al., 2011; Tsurutani & Ho, 1999; Turner et al., 1977; Vasquez et al., 2007; Winterhalter et al., 1994, 1995, 2000). MDs were earlier called "magnetic holes or MHs." However, there is confusion with this term, and we suggest to the reader that MD is a better name for this phenomenon. The presence of many MDs in the interplanetary medium clearly indicates that the solar wind is highly "compressive" (here at this stage in the development of this topic we only indicate that the magnetic field is not constant. We will address whether it is compressive in an adiabatic sense later. This is a different meaning of the word "compressive" as discussed previously for cometary magnetosonic waves). Also note that, although there are many magnetic field magnitude

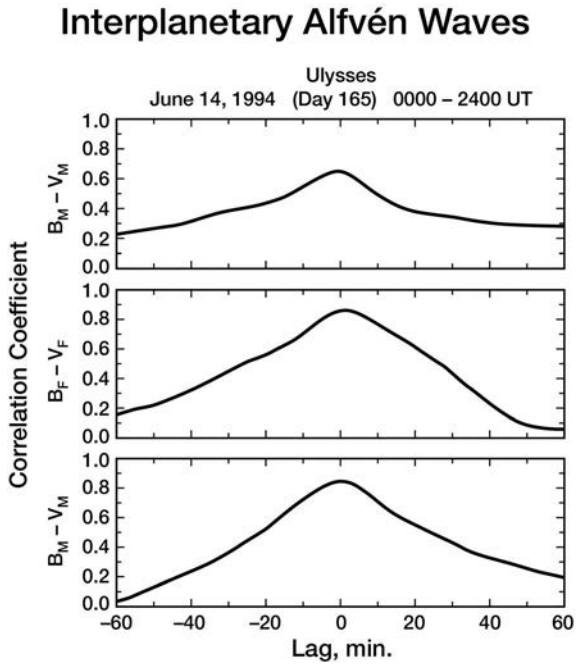


**Figure 11.** Cross correlation of $V_R$-$B_R$, $V_T$-$B_T$, and $V_N$-$B_N$ for the day of 14 June 1994. Taken from Tsurutani et al. (1996).

decreases, there are very few magnetic field magnitude increases of comparable magnitude to the decreases. This latter topic will be addressed further later in this paper.

To identify the nature of the magnetic field and velocity fluctuations in Figure 10, we apply the Belcher and Davis (1971) method of analysis for identifying Alfvén waves, looking at the cross-correlation between the components of the magnetic field and velocity components. The results for an examination of 1 day of the data in Figure 10 are given in Figure 11. In Figure 11 it is shown that three *R*, *T*, and *N* component correlation coefficients peak at zero lag, indicating that the fluctuations are Alfvén waves propagating outward from the Sun.

It should be apparent to the reader that these waves are not your "textbook" Alfvén waves where the analogy of the waves is a small-amplitude transverse pluck of a taut string. Release of the string launches transverse Alfvén waves propagating in both directions along the string. Here the entire magnetic field is oscillating up and down (and sideways as well)! The interplanetary Alfvén waves are of very large amplitude and highly nonlinear.

One important point indicated by one referee is that the correlation coefficients between the various Bi and Vi components at zero lag are high but never reach values of 1.0. The reason for this has not been explained. It could be caused by some nonlinear wave evolution or by other wave modes present in the interplanetary medium. For the interested reader we refer them to Glassmeier et al. (1989) for a discussion of comet Halley coherency spectrum.

### 2.4. Interplanetary Discontinuities

There are four basic types of discontinuities. These are listed in Table 1. They are rotational (RD) and tangential (TD) discontinuities, shocks (S), and contact discontinuities (CDs) (see Landau & Lifschitz, 1960). RDs have nonzero magnetic normal components, and for isotropic plasmas, the transverse component of *H* is constant across the discontinuity surface ($H_t = 0$). Ideally, RDs have large normal components and little change in magnetic field magnitude. TDs have a lack of a magnetic field normal across their surfaces ($H_n = 0$). Shocks have mass flow across their surfaces, and the magnetic field normal and tangential components need not be conserved. CDs are discontinuities where the magnetic fields are identical on both sides, but the plasmas differ in temperature and density. There is no mass flow across the surface.

Hsieh et al. (2014) have possibly identified one CD event occurring in interplanetary space. However, because CDs occur so infrequently (they have been rarely detected), they are not pertinent to the discussion of interplanetary turbulence here.

**Table 1**
*Discontinuity Properties*

| | Mass flux | Change in magnetic field |
|---|---|---|
| Type of discontinuity | $\rho V_n$ | $\underset{[H]}{\rightarrow} = 0$ |
| Rotational discontinuity | ≠0 | $[H_t] = 0\ H_n \neq 0$ |
| Tangential discontinuity | 0 | $\underset{[H_t]}{\rightarrow} \neq 0\ H_n = 0$ |
| Shock | ≠0 | $\underset{H_t}{[\rightarrow]} \neq 0\ H_n \neq 0\ [H_t] \neq 0$ |
| Contact discontinuity | 0 | $\underset{[H_t]}{\rightarrow} = 0\ H_n \neq 0$ |

*Note*. Taken from Tsurutani, Glassmeier, et al. (1997).

### 2.5. Shocks in Interplanetary Space

There are three types of MHD shocks: fast (magnetosonic), intermediate (Alfvénic), and slow (sonic). These are discussed in detail in Kantrowitz and Petschek (1966), Kennel et al. (1985), and Tsurutani, Lakhina, Verkhoglyadova, Gonzalez, et al. (2011). Fast shocks have speeds relative to the ambient solar wind plasma that are faster than the local magnetosonic speed. Intermediate shocks have speeds in between the intermediate MHD wave and the magnetosonic wave speeds, and slow shocks have speeds greater than the MHD sonic speed and less than the intermediate MHD wave speed. All shocks can be further subdivided into forward and reverse, as mentioned earlier.

Interplanetary scientists have been able to identify these various types of shocks and their properties through detailed data

analyses. Colburn and Sonett (1966) and Abraham-Shrauner (1972) were among the first to develop data analysis techniques which are still in use today. Colburn and Sonett (1966) used magnetic field data alone (magnetic coplanarity) to identify the normal directions for shocks. The Abraham-Schrauner technique uses both the magnetic field and the plasma data. This has therefore been called the "mixed-mode" method. However, it should be mentioned that the two methods give slightly different results (Tsurutani & Lin, 1985). The causes for this discrepancy have not been solved at this time. Once the normal directions of the shocks have been established, the Rankine-Hugoniot conservation equations are applied to obtain the shock speeds in the upstream plasma reference frame.

The most frequently observed shocks in the interplanetary medium are fast forward shocks and fast reverse shocks. Some of these shocks are driven by ejecta from the Sun in association with solar flare events. These ejecta were originally called "driver gases" (Tsurutani et al., 1988) but are now called ICMEs (Echer et al., 2008). There are also forward and reverse shocks associated with the boundaries of CIRs (Echer et al., 2010; Smith & Wolfe, 1976; Tsurutani, Smith, Pyle, et al., 1982), as mentioned previously.

Very few well-established cases of slow shocks have been detected in interplanetary space. Thus, Chao and Olbert (1970), Burlaga and Chao (1971), Richter (1991), and Ho et al. (1994) have reported only individual cases. Slow shocks are thus believed to be relatively unimportant as contributors to the power in interplanetary turbulence and will not be discussed further at this time. However, the subject of slow shocks will be brought back somewhat later in this review.

Clearly established intermediate shocks in interplanetary space have not been identified to date. The theoretical possibility of their existence or nonexistence has been debated in the literature (Jeffrey & Taniuti, 1964; Kantrowitz & Petschek, 1966; Wu, 1987). We will come back to the topic of intermediate shocks later in the paper as well.

Figure 12 shows a Climate and Weather of the Sun-Earth System II (CAWSESII) interplanetary interval detected in the ecliptic plane by the Advanced Composition Explorer (ACE) satellite. We show this case to comment on the frequency of fast shocks detected at low latitudes. One would not expect such shocks to occur at high latitudes because solar ARs are confined to ~35° latitudes, as stated before. From the top to bottom of Figure 12 are the solar wind velocity, density, temperature, the three components of the magnetic field (in geocentric solar magnetospheric coordinates), and the field magnitude. The bottom panel is the geomagnetic *Dst* index (Iyemori, 1990). In the geocentric solar magnetospheric system, the **X** axis points toward the Sun, the **Y** axis is in the $\mathbf{\Omega_E} \times \mathbf{X}/|\mathbf{\Omega_E} \times \mathbf{X}|$ direction, and **Z** completes the RH system. In the above, $\mathbf{\Omega_E}$ is the direction of the Earth's south magnetic pole.

Figure 12 shows three examples of fast forward interplanetary shocks. These events are indicated by vertical red lines with a "FS" above them. The FSs are characterized by sharp increases in the solar wind speed, plasma density, plasma temperature, and magnetic field magnitude. For each shock, the above described methods were used to identify their characteristics. The normals were first calculated, the Rankine-Hugoniot relations were applied to get the shock upstream speeds, and a comparison to the upstream magnetosonic speeds was made to get their magnetosonic Mach numbers. Details of the shock properties can be found in Tsurutani et al. (2008). There is also a reverse wave (RS) which is noted to be propagating into the low beta MC (one part of an ICME). The RS was found to be propagating at a speed below the local magnetosonic wave speed and thus was not a shock. It is thought that the RS was once a reverse shock which then propagated into the low beta MC where the local magnetosonic speed is quite high. The MC is indicated by the black horizontal bar. Thus, the speed of the reverse shock fell below the local magnetosonic speed and became a wave. The wave should damp out with further propagation.

The low beta characteristic of a MC is used for its identification (Burlaga et al., 1981; Tsurutani & Gonzalez, 1994). The southward magnetic field component of the MC led to magnetic reconnection (Dungey, 1961) and the resultant magnetic storm indicated by the large negative *Dst* values (Gonzalez et al., 1994).

The MC is thought to drive both the third FS (from the left) and the RS. The other two preceding forward shocks were presumably generated by two other ICMEs, which were not detected by the spacecraft. Multiple flaring occurred at the solar active region (AR), and many ICMEs were launched (Echer et al., 2011). So far "blast wave" shocks (shocks without attached driver gases) have not been detected in interplanetary space. However, it is possible that when one gets closer to the Sun, blast waves may indeed be

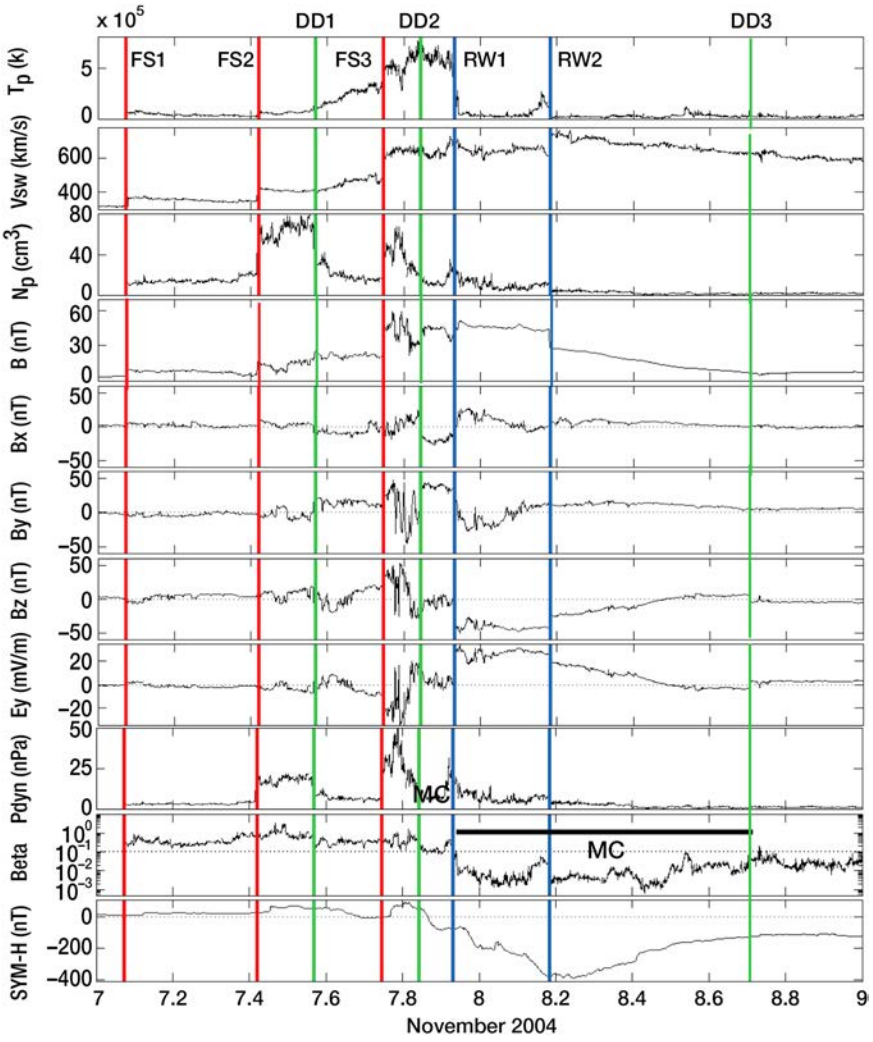


**Figure 12.** Fast forward shocks are denoted by an FS label at the top and vertical red lines. A magnetic cloud is denoted by "MC" and a horizontal green line. An MC is a portion of a driver gas/interplanetary coronal mass ejections. Taken from Tsurutani et al. (2008).

detected. Future observations by Solar Orbiter and Solar Probe Plus and a proposed Icarus mission (Krasnosselskikh et al., 2016) which, if approved, will go even closer to the Sun have the possibility of detecting blast wave shocks.

Figure 12 shows three FSs detected on 7 November 2004. This relatively high occurrence rate is unusual. This anomalously high shock occurrence rate was due to the condition that a very prolific AR was present at the Sun and was facing the Earth. A more normal fast shock occurrence rate at 1 AU is approximately one per week.

Interplanetary shocks (such as in Figure 12) at ~1 AU are relatively weak. Typical magnitudes are (magnetosonic) Mach numbers of 1 to 3 (Echer et al., 2010, 2011; Tsurutani & Lin, 1985). It should be noted that this example was taken from in-ecliptic data. There should be even far fewer fast mode shocks in high-speed solar winds, the topic of this study. Thus, fast shocks are also not particularly important for interplanetary power spectra of solar wind HSSs.

### 2.6. Rotational and Tangential (Directional) Discontinuities and Their Occurrence Rates in High-Speed and Slow-Speed Streams

The two remaining structures in the interplanetary medium which can add significant "power" to the turbulence are RDs and TDs. These are schematically shown in Figure 13. A TD is shown on the left. For TDs, the magnetic field direction and magnitude on either side can be different, but by definition, there is no

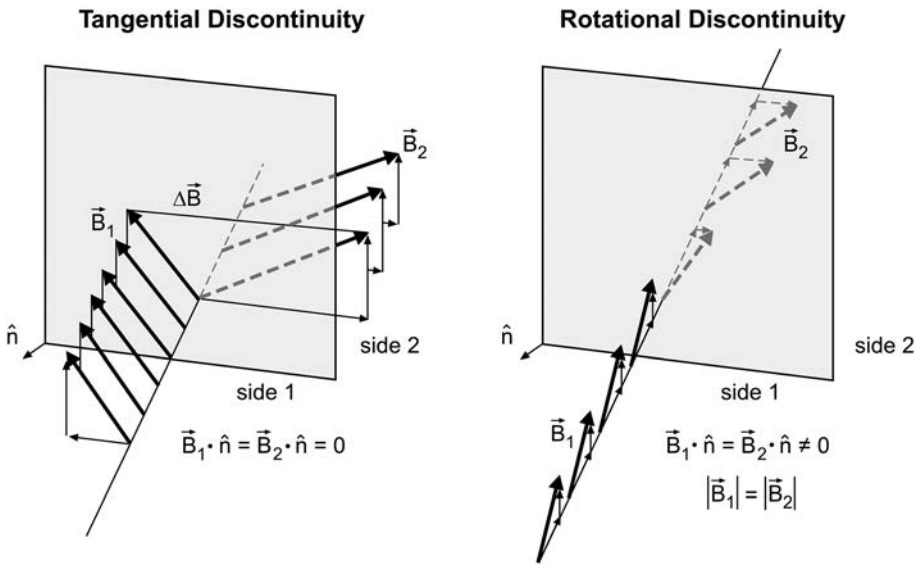


**Figure 13.** A schematic of a (left) tangential discontinuity and a (right) rotational discontinuity. The plane shaded in gray represents the discontinuity surface. The figure was taken from Tsurutani, Glassmeier, et al. (1997).

magnetic component normal to the discontinuity surface. An RD is shown on the right. The magnetic field has a sharp "kink" at the discontinuity surface. This is a sharply crested Alfvén wave.

There have been and continue to be arguments in the scientific community on the relative number of TDs and RDs (Belcher & Solodyna, 1975; Burlaga et al., 1977; Horbury et al., 2001; Knetter et al., 2004; Lepping & Behannon, 1980; Neugebaueer & Giacalone, 2010; Neugebauer, 2006; Neugebauer et al., 1984; Smith, 1973a; Tsurutani et al., 2007). RDs are structures which contribute to wave power in the turbulence power spectra. However, TDs are not waves but still are measured by power spectra. TDs are static structures, which, if they exist, should be removed from the values of the power. Unfortunately, to date, no one has devised a method to identify the "collective power" associated with TDs to extract it from overall power spectrum. However, one might apply a wavelet transform to remove such structures as Salem et al. (2009) have done for intermittent structures.

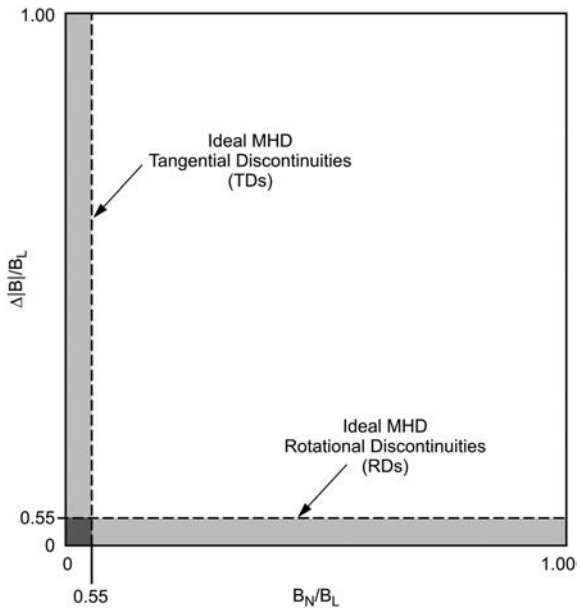


**Figure 14.** Discontinuity phase space diagram. Tangential discontinuities align along the vertical gray strip, rotational discontinuities along the horizontal gray strip, and discontinuities with both properties in the dark square near the origin. Fast shocks will appear in the white area.

In 1973, Smith (1973a, 1973b) devised a means of separating TDs from RDs, using a discontinuity phase space diagram as shown in Figure 14. All "directional discontinuities (DDs)" were first identified by sharp changes in the magnetic field direction (DDs can be either RDs or TDs or shocks). For the phase space plot, the normal magnetic field component $B_n$ and the change in magnitude $|\Delta B_0|$ were calculated. Both of these values were then "normalized" by dividing by the larger magnetic field magnitude on either side of the discontinuity, $B_L$. In Figure 14, the vertical axis is $|\Delta B_0|/B_L$ and the horizontal axis is $B_n/B_L$. Thus, all discontinuities can be plotted in this $1.0 \times 1.0$ phase space. Ideal TDs lie in the gray vertically aligned area. Ideal TDs lie in the gray horizontally aligned area. The dark square near the origin identifies discontinuities that have properties of both TD and RDs. Shocks will appear in the white area. This method sometimes works well in distinguishing RDs from TDs (Neugebauer, 1984; Smith et al., 1973a, 1973b).

There have also been questions about the occurrence frequency of DDs in slow-speed streams and HSSs. This is an important question because a lot of the magnetic turbulence power must be associated with discontinuities as mentioned earlier. Some simple computer programs were written to automatically detect DDs and to

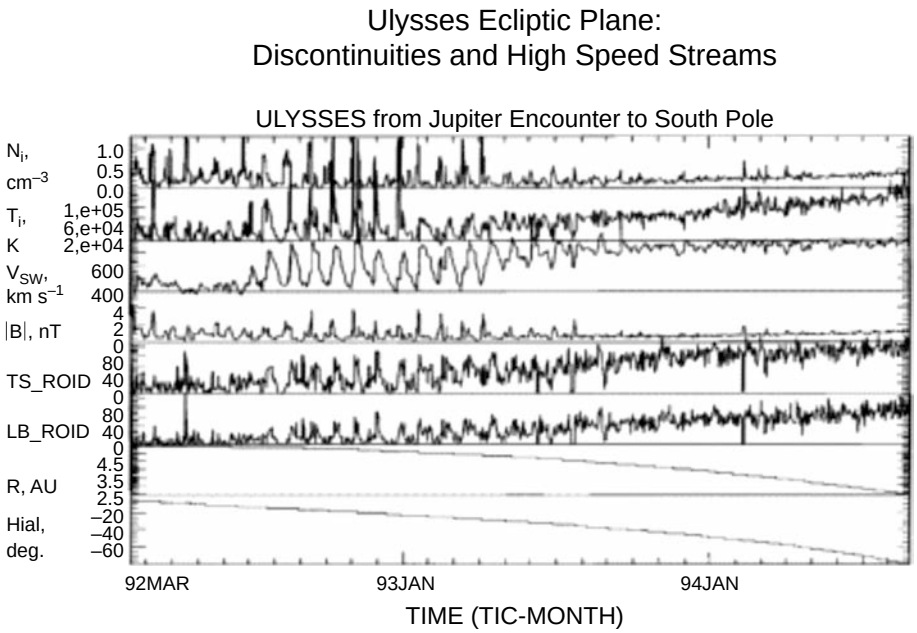


**Figure 15.** Directional discontinuity (DD) rate of occurrence (discontinuities/d) for the Ulysses ecliptic plane traversal from 1 to ~5 AU, and then to large negative heliospheric latitudes (and slightly lower heliospheric distances). The rate of interplanetary discontinuities is lowest in slow-speed solar wind streams and a factor of ~2 to 3 times higher in high-speed streams. Taken from Tsurutani et al. (1996).

determine their rates of occurrence. Tsurutani and Smith (1979) used the criteria $\Delta\mathbf{B}/B_L > 0.5$, and Lepping and Behannon (1986) used a slightly different criteria $\theta = \text{cosine}^{-1}\ (\mathbf{B}_1 \cdot \mathbf{B}_2/|\mathbf{B}_1||\mathbf{B}_2|) \geq 30°$.

Tsurutani et al. (1996) used both methods to apply to the Ulysses magnetic field data. The results are shown in Figure 15. From top to bottom are the solar wind density, temperature, velocity, and magnetic field magnitude. The fourth and fifth panels from the top are the rate of interplanetary discontinuities (ROID) values for the Tsurutani and Smith criteria and Lepping and Behannon criteria, respectively. The bottom two panels give the spacecraft location in radial distance from the Sun and heliospheric latitude, respectively.

The primary results pertinent to this paper are given in the third, fifth, and sixth panels from the top. When the solar wind has velocities near ~400 km/s (slow solar wind), the ROID values are lowest. In HSSs with speeds near ~800 km/s, the ROID rates are a factor of ~2 or 3 times higher. An "oscillation" between low-speed streams and HSSs occurs during the interval between August 1992 and May 1993. The cause of this oscillation is due to a "finger" of the south polar coronal hole extending up to higher latitudes. As the Sun rotates, the normal to the finger occasionally points toward the spacecraft and the HSS emanating from the coronal hole "finger" flows radially outward and eventually engulfs the spacecraft. As the Sun rotates away, so does the HSS. The stream recurs at Ulysses at the solar rotation period of ~25 days.

From October 1993 until September 1994, the spacecraft was totally immersed in the HSS as Ulysses reached sufficiently negative latitudes. The ROID rate also no longer shows an ~25 day oscillation. The Tsurutani and Smith method gives a near-constant rate of ~80 discontinuities/d, and the Lepping and Behannon method gives a near-constant rate of ~65 discontinuities/d when Ulysses was totally in the HSS.

There is clearly a higher rate of DDs in the HSSs compared to the rate in slow-speed streams. Assuming that the discontinuities are essentially of the same nature in both types of streams with similar individual DD "power," this indicates that higher DD power exists in the HSSs. This may partially explain the higher value of the power spectra shown in Figure 1. Of course, Alfvén wave power may contribute as well.

### 2.7. The Nature of Interplanetary Alfvén Waves From a Single Wave Viewpoint

Figure 16 shows a typical Alfvén wave detected in the interplanetary medium. We will examine this wave in the same manner that was done for a cometary magnetosonic wave in section 2.2. However, because this is a nonlinear Alfvén wave and not a magnetosonic wave, we can assume that the wave evolution and properties might be quite different.

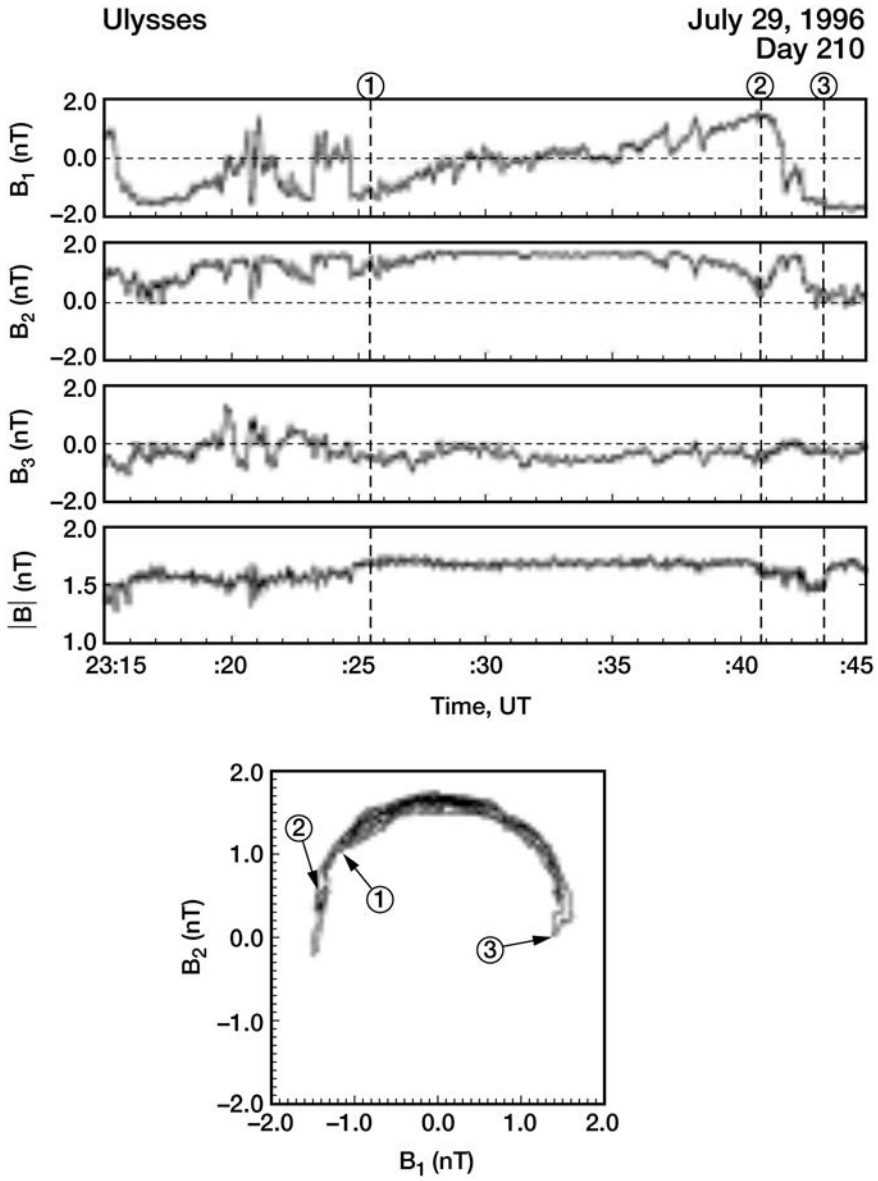


**Figure 16.** An "arc polarized" Alfvén wave. The wave perturbation vector rotates slowly from point (1) to point (2) and then rapidly back from point (2) to point (3). The B1-B2 hodogram at the bottom shows the "arc" rotation. Taken from Tsurutani et al. (1994).

The magnetic field is plotted in the top panel in minimum variance coordinates where the 1, 2, and 3 subscripts designate the field component in the maximum, intermediate, and minimum variance directions, respectively. The top three plots are the field components, and the bottom is the field magnitude.

In Figure 16, a 360° cycle of an Alfvén "wave" is indicated by vertical lines identifying the start of the wave at (1), an intermediate step at (2), and the end of the wave at (3). If one examines the B1 (top) panel, it can be noted that the magnetic field component slowly increases from ~−1.6 nT to ~+1.7 nT from points (1) to (2). There is little or no variation in the B2 and B3 components during this interval. The magnetic field magnitude remains constant at a value of ~1.7 nT throughout this portion of the wave oscillation. This is a point that we will come back to later. From points (2) to (3), the B1 component makes a sharp change from ~+1.7 nT to ~−1.7 nT. This sharp change brings the field back to its initial orientation.

The bottom panel shows the B1-B2 wave hodogram for the whole time interval shown in the top panel. The points (1) to (3) are indicated in the plot. Here the "arc" polarization (Riley et al., 1995, 1996; Tsurutani et al.,

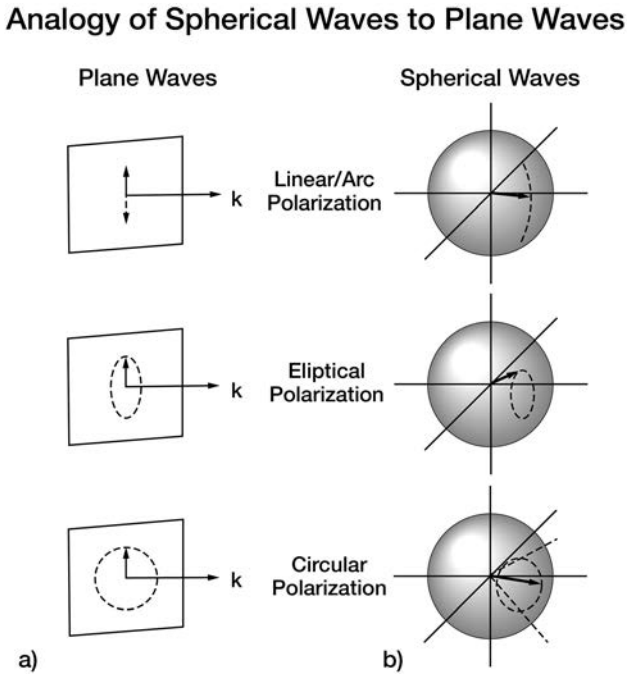


**Figure 17.** An analogy between (left) planar waves and (right) spherical waves. (top to bottom) Three types of wave polarization are shown. Taken from Tsurutani, Ho, et al. (1997).

1994; Tsurutani, Smith, et al., 1995; Tsurutani & Ho, 1999) can be clearly seen. The wave rotates from points (1) to (2) in an arc, and then back from points (2) to (3), also in an arc.

This Alfvén wave is "phase-steepened" very much like the large-amplitude nonlinear cometary wave shown previously. As previously mentioned, phase-steepening means that the wave does not have an even rate of wave phase rotation with time (or distance) like a sinusoidal wave does. The rotation is concentrated on a steepened end (in this case, the antisunward end). There is a ~180° phase rotation from points (2) to (3). Thus, the wave is effectively separated into two parts: a phase-steepened portion with ~180° of phase rotation and the trailing part with the remainder of ~180° of phase rotation.

There are both similarities and differences between the Alfvén wave phase-steepening process and that of a cometary magnetosonic wave. As the Alfvén wave phase-steepens, it is creating high-frequency power. This is similar to the cometary magnetosonic wave. The remaining part of the Alfvén wave is evolving into low-frequency power. This too is similar to the magnetosonic wave evolution. However, the magnetosonic wave carries RH polarized helicity. The Alfvén wave does not. Another difference is that Alfvén wave stops at ~180° phase rotation for the steepened edge and the cometary magnetosonic wave apparently does not.

The phase-steepened edge of the Alfvén wave contains high-frequency wave power. Has this wave "broken"? We will discuss this topic later in the paper.

The trailing portion of the wave carries ~180° phase rotation. Now this phase rotation occurs over almost the original Alfvén wavelength, so the wave period has essentially doubled. We use the term "period doubling" to describe this phenomenon. This is similar to the cometary magnetosonic wave. This is not the familiar use of the term in weak turbulence, but here, it is descriptive of nonlinear wave evolution and seems like an appropriate term to use.

An obvious question raised by the above discussion is what is "arc polarization" and what does it mean in a physical sense? In Figure 17, the left-hand column shows various polarizations of plane waves. From top to bottom are circular polarization, elliptical polarization, and linear polarization. The RH side of the figure shows perturbation vectors rotating on the surface of a sphere. If the magnetic field magnitude is constant throughout the wave (as B1 from points (1) to (2) in Figure 16), the wave perturbation vector is confined to rotate on a surface of a sphere. The top figure shows a rotation in a circular sense. The second figure has a rotation in an elliptical sense. However, it is clear that there cannot be a rotation which has a linear sense. This can occur only for small-amplitude waves, and even then, there is still some "arc" present. Thus, our interpretation of interplanetary arc-polarized Alfvén waves is that they are spherical waves.

Spherical waves, by definition, are not plane waves. Why are (some) interplanetary Alfvén waves spherical in nature? One possibility is that the waves have been detected close to their source. This will be discussed further later in the paper.

### 2.8. Magnetic Decreases and Alfvén Waves

Earlier in Figure 10 we showed 30 days of Ulysses magnetic field data within a high-speed solar wind stream. There were many MDs in the data, while there were very few magnetic field increases. We will explore the possible physical causes of MDs in this section. One thing to note in Figure 10 is that the "compressional power" shown in Figure 1 must be mainly due to the presence of MDs in the high-speed solar wind.

There have been many proposed causes of MDs. Baumgärtel (1999) has suggested that MDs could be the dark soliton solutions of the Derivative Nonlinear Schrodinger equation. However, the applicability of the Derivative Nonlinear Schrodinger equation for highly obliquely propagating nonlinear waves has been questioned by Buti et al. (2001). Buti et al. (2001) have suggested an alternative mechanism: local inhomogeneities introduced by large-amplitude Alfvén wave packets that evolve into MDs.

Sakai et al. (2005) have analyzed the nonlinear dynamics of a shear Alfvén wave using a 2D3V PIC simulation code. They find conditions when the Alfvén wave becomes unstable to the modified two-stream instability with quasi-electrostatic lower-hybrid wave generation and electron heating in the ambient magnetic field direction. As the shear wave becomes unstable, ion acoustic waves are excited, resulting in ion heating.

Roytershteyn et al. (2015) have performed a 3-D kinetic simulation of decaying turbulence. The authors have found MDs which are pressure balanced structures that have a tendency to align along the mean magnetic field direction. The decrease in magnetic pressure is found to be due to electron perpendicular pressure.

Although not directly relevant to high-speed solar wind streams, we mention several other major proposed mechanisms for interplanetary MD formation. Tsubouchi and Matsumoto (2005) have modeled interplanetary RD interactions with the Earth's bow shock with resultant MD formation. In their simulation, proton parallel heating occurs from enforced conversion of proton perpendicular motion into parallel motion by the imposed rotational magnetic field. The resultant intense parallel/antiparallel flows are believed to generate the field gradient at the edges, acting as a mirror force reducing the magnetic intensity.

Vasquez and Hollweg (1999) and Vasquez et al. (2007) have suggested that wave-wave interactions in the turbulent sheaths behind interplanetary shocks could create MDs. Their idea is that MD generation occurs when a pair of oppositely traveling Alfvén waves generates pressure-balance structures.

Tsubouchi (2009) has used a 1-D MHD simulation to show that Alfvénic fluctuations in the HSS interacting with a velocity gradient structure will form MDs. The initial Alfvén wave disintegrates into two Alfvén modes traveling in opposite directions. The field components are amplified when passing through the magnetic compression region, causing a local current reversal. The resulting force sweeps the plasma backward to form a pressure increase and the MD.

Although the above theoretical discussions pertain to MD generation, single wave observations indicate that the interplanetary MDs in high-speed solar wind streams are related to Alfvén waves. We will follow the discussion of MD generation below, but with further observational information.

Figure 18 shows the typical relationship between Alfvén waves and MDs. The format of Figure 18 is similar to that in Figure 16. The panels from top to bottom are the B1, B2, and B3 components in minimum variance coordinates and magnetic field magnitude. There are three Alfvén wave cycles present in the figure. The bottom panel is a B1-B2 hodogram of the middle wave. There is a schematic of the hodogram on the bottom right.

The three phase-steepened Alfvén waves are most apparent in the B1 component. The cycles are denoted by the sawtooth-like variations in this magnetic field component. The hodogram shows that the middle wave is arc-polarized. MDs are located at the phase-steepened edges of the Alfvén waves. These are denoted by vertical dashed lines. The MDs can be noted in the magnetic field magnitude plot.

The question of what MDs are and if they are part of the Alfvén wave itself has been addressed by many researchers (Baumgärtel, 1999; Buti et al., 1998, 2001; Dasgupta et al., 2003; Hellinger et al., 2017; Neugebaueer & Giacalone, 2010; Tsubouchi, 2009; Tsubouchi & Matsumoto, 2005; Tsurutani, Galvan et al., 2002; Tsurutani, Dasgupta, et al., 2002; Tsurutani et al., 2003; Tsurutani, Lakhina, et al., 2005; Tsurutani, Lakhina, Verkhoglyadova, Echer, et al., 2011; Vasquez et al., 2007; Vasquez & Hollweg, 1999). All of the above ideas about MDs are that they are structures that are created or are associated with the Alfvén waves but are not an intrinsic part of the wave itself. We will show some observational evidence that will indicate the nature of these important plasma structures.

Figure 19 shows the phase space plot of 129 randomly selected MDs detected within the south solar polar HSS. Only cases where the MD magnetic field magnitude changes ($\Delta|B|/B_L$) were greater than 0.2 were analyzed. This format is the same as in Figure 14. It is noted that the MDs not only have large magnitude changes (up to 90%) but they can also have large normal components as well.

Assuming that solar wind protons have a bi-Maxwellian temperature distribution, the perpendicular (to the ambient magnetic field) and the parallel temperatures were derived for 32 MD events detected in an HSS. Temperature measurements both inside the MD and then at a point just outside the MD were obtained. The values of the ratio of the inside to outside temperatures are shown in Figure 20. The top panel is the perpendicular temperature inside-to-outside ratio distribution. The bottom panel is the parallel temperature inside-to-outside ratio distribution.

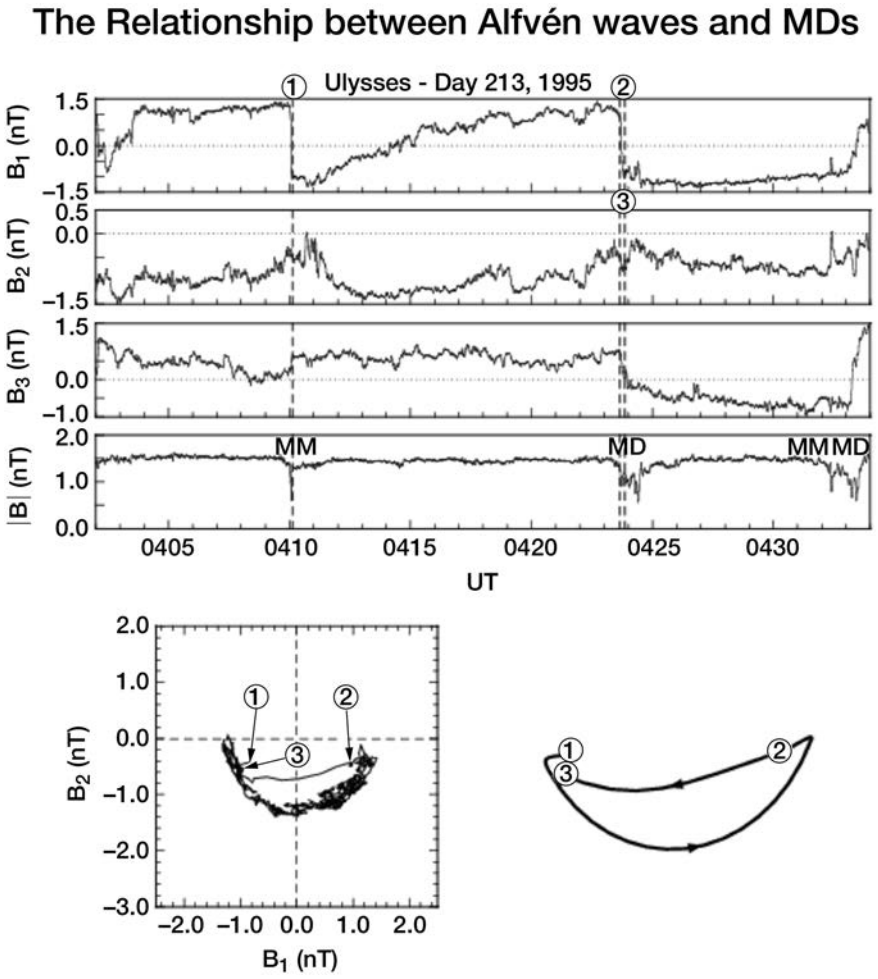


**Figure 18.** Phase-steepened Alfvén waves and magnetic decreases. The figure is taken from Tsurutani, Galvan, et al. (2002).

The top panel of Figure 20 shows that the ratios of the perpendicular temperature inside the MD to that outside the MD are mostly >1.0. The bottom panel shows that the ratio of the parallel temperature inside the MD to that outside is centered at ~1.0. It is clear that perpendicular heating (top panel) is occurring for the plasma within the MDs. Similar results indicating perpendicular ion heating have been shown by Fränz et al. (2000) and Neugebauer et al. (2001).

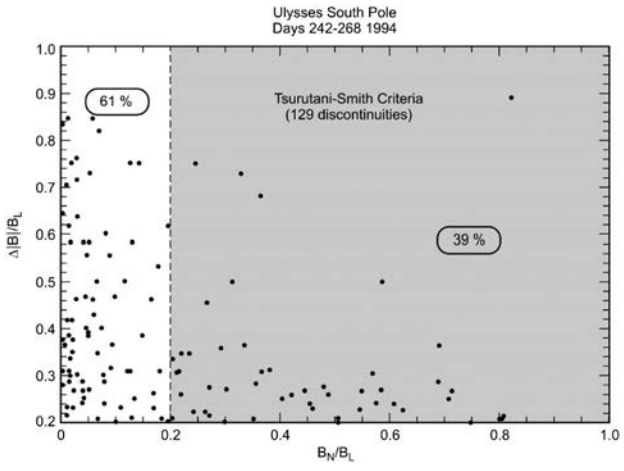


**Figure 19.** The Smith (1973a, 1973b) method applied to magnetic decreases in a high-speed stream. The figure is taken from Tsurutani and Ho (1999).

Tsurutani, Dasgupta, et al. (2002) took the analysis one step further. If there is local heating occurring, then could there possibly be observable dissipation in the form of waves associated with plasma instabilities? Tsurutani, Dasgupta, et al. (2002) identified mirror mode structures and ion cyclotron waves within MDs. Proton temperature anisotropies with $T\perp/T_{||} > 1$ are necessary for the mirror instability to grow (Genot et al., 2009; Hasegawa, 1969; Hasegawa & Tsurutani, 2011; Hellinger, 2007; Hellinger et al., 2017; Pokhotelov et al., 2008; Price et al., 1986; Travnicek et al., 2007; Tsurutani, Lakhina, Verkhoglyadova, Echer, et al., 2011; Tsurutani, Smith, Anderson et al., 1982; Volwerk et al., 2008, 2016). The same anisotropy is necessary for the proton temperature anisotropy instability to grow (Gary et al., 1993; Kennel & Petschek, 1966; Remya et al., 2013). Remya et al. (2013, 2017) have clarified that it is the electron anisotropy and plasma β that distinguish which of the two modes dominate.

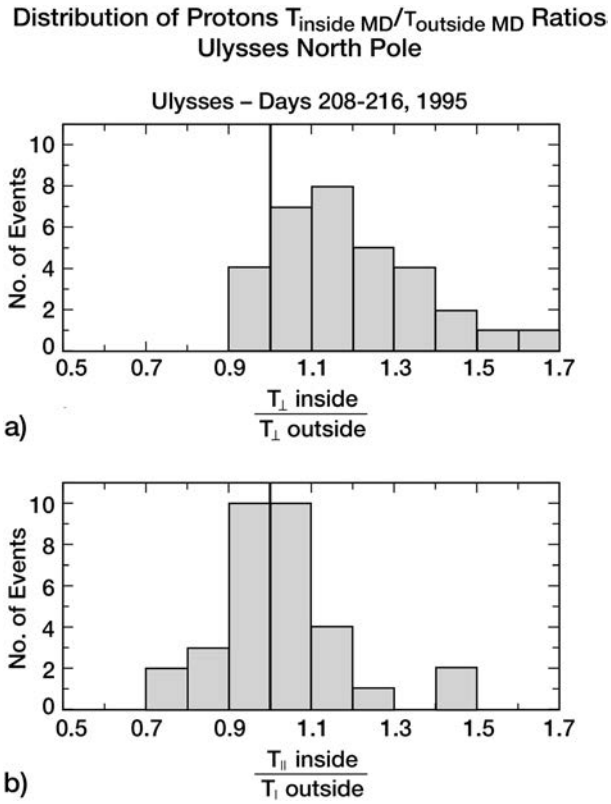


**Figure 20.** The proton (top) $T\perp$ temperature inside-to-outside ratio distribution and (bottom) $T_{||}$ temperature inside-to-outside ratio distribution. Taken from Tsurutani, Dasgupta, et al. (2002).

Additionally, electron-associated plasma waves have been detected inside MDs. Lin et al. (1995, 1996) and MacDowall et al. (1996) have detected electron whistler mode waves and longitudinal Langmuir waves inside MDs. Whistler mode waves are generated by an electron temperature $T\perp/T_{||} > 1$ anisotropy instability (Kennel & Petschek, 1966; Tsurutani & Lakhina, 1997). Langmuir waves are generated by an electron beam instability.

Dasgupta et al. (2003) and Tsurutani, Dasgupta, et al. (2002) have suggested that it is the steepened edge of the Alfvén wave and the pondemotive force associated with it that is responsible for proton and electron acceleration/heating. As discussed previously, the Buti et al. (2001), Sakai et al. (2005), and Roytershteyn et al. (2015) mechanisms could also be operative. Saito et al. (2015) have indicated that nonlinear dissipation of a finite amplitude whistler wave at ion scales could heat the ions. Current observations are not good enough to determine which, if any, of the hypotheses are correct. However, in any of the above scenarios, the Alfvén waves are dissipating kinetically.

It should be noted that, although these various types of plasma waves (ion and electron cyclotron, mirror mode, and Langmuir waves) have been detected inside MDs, the waves lasted only short time durations. The amount of power would be negligible in the overall interplanetary power spectrum.

What created the MDs? Tsurutani, Dasgupta, et al. (2002) have proposed that it is the heated ions and electrons accelerated by the ponderomotive force that have created the high β MD regions. Much of the ambient magnetic field is pushed out of the region into the neighboring areas. An alternative suggestion is that MDs are the exhaust fans of interplanetary magnetic reconnection (Neugebaueer & Giacalone, 2010). If the latter suggestion is correct, that would explain the presence of slow shocks at the boundaries of the MDs (Farrugia et al., 2001). In either scenario, the heated plasma is the source for the MDs. There are no large positive pulse magnetic fields, only negative pulses or decreases.

A multispacecraft spatial study was performed on MDs in the ecliptic plane to determine if the structures were evolving within short distances. This was done using the ACE spacecraft, which was located near the L1 libration point, ~0.01 AU upstream of the Earth (along the Sun-Earth line), and one of the 4 Cluster spacecraft orbiting the Earth. A similar study is not possible to do at high latitudes because neither NASA nor the European Space Agency has two satellites spaced close to each other in these locations.

Figure 21 shows the same MD detected at ACE on the left and the four Cluster spacecraft on the right. The measured solar wind speeds were used to calculate convection times in order to identify the same MD. This event occurred on day 50, 2001. The four Cluster spacecraft are located relatively close to each other, namely, $<1$ $R_E$ (6,378 km); thus, the profiles of all magnetic fields look essentially the same (the solar wind propagation delay times have been removed). The coordinate systems of the MD at ACE and Cluster are the same, RTN. The ACE horizontal axis (time) has been compressed to allow both panels to be placed on the same figure. There are similarities in the variations of the *R*, *T*, and *N* field components between ACE and Cluster (this is the steepened edge of the Alfvén wave and a "discontinuity" shown in high time resolution), but there are differences as well. The most significant and noticeable difference is in the scale of the *B* magnitude for the MD. The MD 1/e beginning and end are ~2155:33 and ~2156:16 UT or a duration of ~33 s at ACE. For Cluster the 1/3 beginning and end are ~2306:08 to ~2306:13 UT or an ~5 s duration. The minimum magnetic field in the ACE MD is ~2.3 nT and that for Cluster is ~0.7 nT. So the MD has become much narrower spatially and deeper in minimum magnetic field magnitude at Cluster.

This spatial/temporal size of the MD was different at ACE and at Cluster, indicating rapid evolution within ~0.01 AU. To ensure that this was not some statistical variation, several more MDs were studied in a similar

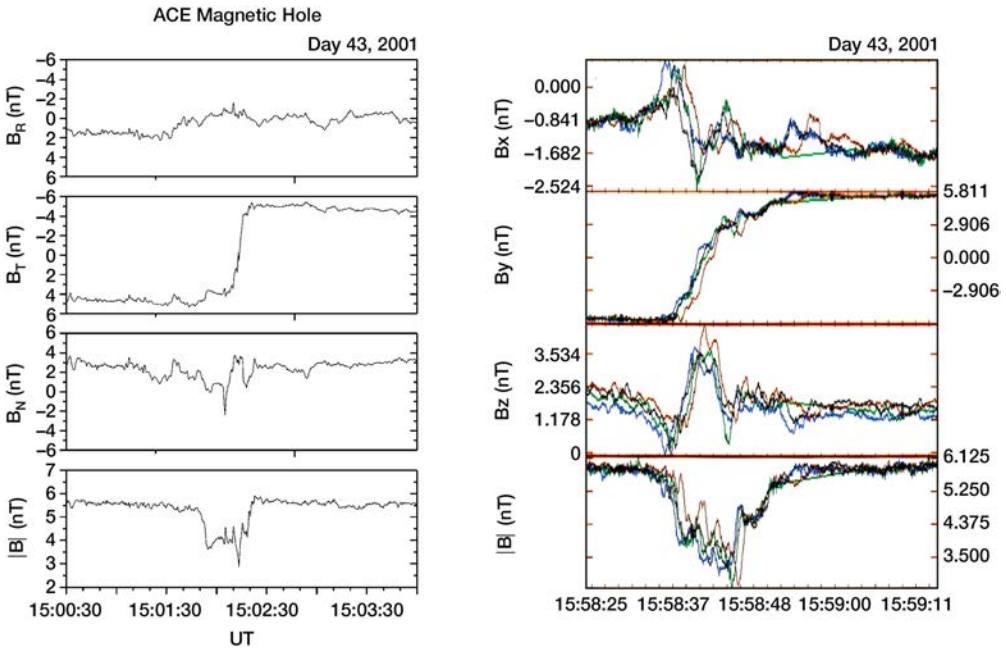


**Figure 21.** A magnetic decrease (MD) detected at the Advanced Composition Explorer (ACE) spacecraft at the L1 libration point and at the 4 Cluster spacecraft orbiting the Earth. The MD is shown in the radial-tangential-normal coordinate system in both panels. The panel on the left (ACE) has been compressed in time to allow it to be placed in the figure.

manner. Table 2 shows the ratio of convection times of seven MD events across ACE to that across the Cluster spacecraft. The solar wind speed was constant for all of the events studied. The events all occurred in 2001. The first column indicates the day of the event and the RH column the ratio of the sizes.

The ratios of MD size at ACE to Cluster vary from 4.4 to 21.3, indicating that in all cases the MDs were decreasing in size while being convected over a short distance of ~0.01 AU, implying that the MDs were evolving quite rapidly. The previous finding that Alfvén waves can be arc-polarized spherical waves is consistent with this picture.

If the MDs are varying rapidly in time (and convected distance), this implies the rapid dissipation of interplanetary Alfvén wave energy. If this is occurring, then why does not spacecraft instrumentation detect rapidly decreasing wave power as a function of distance from the Sun? The authors do not have an answer to this at this time. However, we will address the issue of local generation of the waves in a later section.

## 3. Summary of Alfvén Wave and MD Observations

We have examined high-speed solar wind turbulence from a point of view of single Alfvén wave cycle evolution. Alfvén waves phase-steepen forming an arc of ~180° phase rotation at one edge. Since the nonlinear processes cause the phase rotation to occur in a small spatial region, this is the creation of high-frequency turbulence. At the same time, the lengthening of the remaining part of the wave creates lower frequency turbulence. Both processes are occurring at the same time. We can think of this as "wave breaking" and "period doubling," respectively. Although the term "wave breaking" is most often known for ocean waves approaching a beach, it has also been applied to nonlinear cometary magnetosonic waves (and shocks) discussed earlier. The same basic evolution is occurring with interplanetary Alfvén waves, and we use the term here. "Period doubling" has been used in nonlinear processes, but here, we use it in a highly nonlinear sense. It is an observational feature that best describes nonlinear Alfvén wave evolution. Since interplanetary Alfvén waves are composed of all wavelengths, this turbulence evolution is most probably occurring at all scales down to the proton gyroradius (discontinuity) scale size.

Almost all of the turbulence power (Figure 1) in HSSs between $10^{-1}$ and $10^{-4}$ Hz is associated with the nonlinear Alfvén waves. The Alfvén waves are continually evolving. They are steepening and also dissipating. One

**Table 2**
*Seven Magnetic Decrease (MD) Events Detected at Both the Advanced Composition Explorer (ACE) and Cluster Spacecraft*

| Rate of phase steepening | |
|---|---|
| Event (day) | MD-ACF/MD Cluster |
| 33–34 | — |
| 43 | 4.4 |
| 50 | 5.8 |
| 51(a) | 5.0 |
| 51(b) | 14.5 |
| 76–77 | 21.3 |
| 77 | 5.5 |

*Note*. The event days are given in the left-hand column and the ratio of duration times in the right-hand column. This is taken from Tsurutani, Guarnieri, et al. (2005).

by-product is the MDs. These are believed to be static structures and not waves. Thus, the interplanetary high-speed turbulence is a combination of both propagating waves and static structures.

The extreme value cases of intermittency (Frisch, 1995; Verma, 2004) have been shown to correspond to the formation of coherent structures (Chen et al., 2014; Matthaeus et al., 2015). The coherent structures may be the arc-polarized portions of the Alfvén waves reported here.

The greater occurrence frequency of the DDs as Ulysses went from the ecliptic plane to higher heliographic latitudes can explain the greater amount of spectral power in HSSs, as shown in Figure 1, at least for the high-frequency components. It is presumably the evolution of the Alfvén waves that lead to both greater low-frequency and high-frequency wave power away from the original wave frequencies.

The presence of MDs makes the interplanetary medium highly "compressive." Here we mean that the magnetic field magnitude is not constant. A greater concentration of MDs in high-speed solar wind streams could explain the greater compressional turbulence detected at high latitudes found in Figure 1. It should be noted by the reader that caution should be taken when interpreting the results of Elsässer variable analyses (Elsasser, 1950; Marsch & Mangeney, 1987) of the interplanetary medium. If static nonpropagating structures such as MDs are present in the data set, they could be interpreted as a combination of inward and outward propagating Alfvén waves instead of the static structures that they are.

## 4. Source of the Alfvén Waves

It is believed that the stirring of the foot points of magnetic fields by convective motions in the photosphere (granules and supergranules) can generate Alfvén waves at the Sun. Hollweg (2006) in arguing in favor of this viewpoint has also cautiously pointed out difficulties in this interpretation based on scaling arguments. This currently remains an unsolved problem. However, in this paper, we assume that the interplanetary Alfvén waves are generated at or close to the Sun for lack of better alternatives at this time.

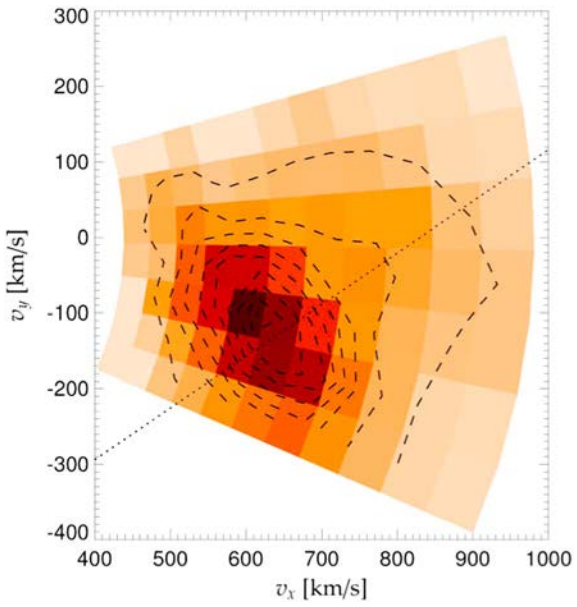


**Figure 22.** The proton distribution function in a high-speed solar wind stream. The dotted line is the magnetic field direction. The red-shaded rectangles indicate the instrument resolution. The figure is taken from Hellinger et al. (2013).

Further from the Sun (>0.3 AU) the association of Alfvén waves with high velocity streams has led to the suggestion that these waves might be generated locally by velocity shear instabilities (Bavassano et al., 1978; Coleman, 1968; Roberts et al., 1987, 1992). The velocity shear of the parallel plasma flow (or proton beams) can generate both electrostatic and electromagnetic low-frequency waves as shown by Dobrowolny (1972, 1977) and Lakhina (1987, 1990).

The solar wind plasma and its embedded magnetic field expand as they propagate from the Sun. Assuming conservation of adiabatic invariants, the plasma should develop a distribution beamed along the magnetic field. Marsch et al. (1982) used the German Helios spacecraft data to study the proton distribution functions in HSSs. The Helios satellite was in orbit around the Sun with a perihelion at ~0.3 AU and an aphelion of ~1.0 AU. It therefore sampled the solar wind at a variety of heliocentric distances. The Helios orbit was in the ecliptic plane.

Marsch et al. (1982) and Hellinger et al. (2013) found a distribution with $T_{\perp}$ much larger than $T_{||}$, opposite to what one might expect. This is shown in Figure 22, taken from Hellinger et al. (2013). The dotted line in the plot is the direction of the interplanetary magnetic field. Matteini et al. (2006, 2007) and Hellinger and Travnicek (2008) have modeled the expanding solar wind and have found that the plasma is

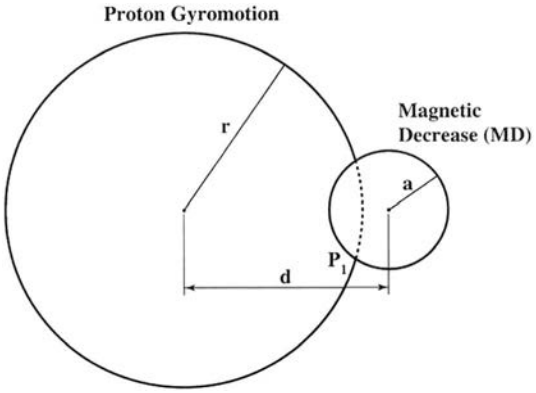


**Figure 23.** A schematic of an energetic proton interaction with an magnetic decrease. The figure is taken from Tsurutani et al. (1999).

unstable to the fire hose and oblique fire hose instabilities at ~1 AU. Of particular interest is that the oblique fire hose instability generates oblique Alfvén waves. For oblique enough magnetic fields (Parker spiral configuration) and conservation of the CGL double adiabatic invariants (Chew et al., 1956), Matteini et al. (2012) find the generation of perpendicular temperature anisotropies (these temperature anisotropies can in turn lead to the growth of MDs and mirror modes). Lower hybrid-type electrostatic instabilities excited by the large-amplitude Alfvén waves (Khazanov et al., 1996; Lakhina et al., 2004; Saito et al., 2015; Sakai et al., 2005) could also create proton anisotropies with $T\perp/T\| > 1$. Such instabilities would heat solar wind protons in the perpendicular direction leading to $T\perp > T\|$. The amplitude threshold for Alfvénic waves exciting these instabilities appears to be lower in low β regions.

Another source of local generation of Alfvén waves is kinetic instabilities associated with the solar wind proton heat flux. Both Ulysses (Goldstein et al., 2000; Matteini et al., 2013) and Helios observations (Marsch and Livi, 1987) indicate a differential streaming between the proton core and beam populations. Hellinger and Travnicek (2011, 2013) have indicated that solar wind expansion leads to an increasing ratio between the differential particle velocity and the local Alfvén speed, also leading to the oblique Alfvén wave instability.

The local generation of interplanetary Alfvén waves, if it indeed takes place, could replenish and add to some of the Alfvén wave energy coming from the Sun, as discussed in section 2.8. Comets passing between the Sun and the Earth can also add to interplanetary turbulence.

## 5. Effects of Interplanetary Turbulence

### 5.1. Energetic Particle Cross-Field Diffusion

There have been many theoretical articles on energetic charged particle diffusion associated with interplanetary turbulence. Some more recent papers are Lazarian et al. (2012), Le Roux et al. (2015), Sun et al. (2016), and Subedi et al. (2017). We direct the interested reader to these papers and their references. A far different mechanism has been proposed which associates energetic particle cross-field diffusion to interactions with MDs. This mechanism is particularly effective for particles with large gyroradii such as solar flare ions. This mechanism is a nonresonant interaction, does not lead to particle acceleration, and does lead to very rapid diffusion. We will briefly review the mechanism.

Figure 23 shows a schematic of an energetic proton with gyroradius *r*, interacting with an MD with a circular cross section radius *a*. The "impact parameter" is *d*. Assuming that the magnetic field is out of the paper, a proton will intersect the MD at point $P_1$.

To illustrate the cross-field diffusion effect, assume that the particle motion is entirely within the plane of the figure and the MD has a tubular geometry such that it is oriented orthogonal to the plane of the figure. There is no effect due to the parallel (into or out of the plane) velocity of the energetic particle. The parallel motion will, however, affect the frequency of encountering of MDs in interplanetary space. This will be addressed later.

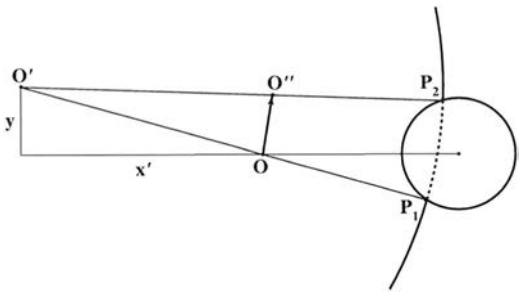


**Figure 24.** Proton gyrocenter displacement from point O to O″ due to the interaction with the magnetic decrease.

Figure 24 shows schematically how the proton interaction with a MD causes motion of the particle's gyrocenter in a direction across magnetic field lines. Taking the example in Figure 23, initially, the particle has a gyrocenter at point O. The particle is gyrating in the ambient magnetic field of strength $B_O$. As the particle hits the MD at point $P_1$, it experiences the lower magnetic field of the MD ($B_{MD}$), and its first adiabatic invariant is broken. Due to the much lower magnetic field magnitude inside the MD, the particle gyroradius is increased (by the factor of $B_0/B_{MD}$) and its new gyrocenter is located at point O′. The particle continues its gyromotion through the MD and exits at point $P_2$ at which time it experiences the

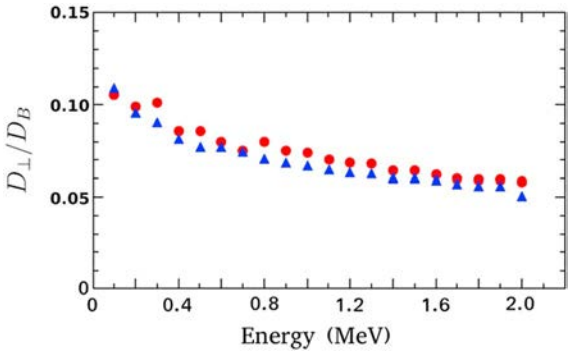


**Figure 25.** The ratio of proton cross-field diffusion ($D\perp$) to Bohm diffusion ($D_B$) as a function of proton kinetic energy. The red dots represent 100 particle-magnetic decrease (MD) interaction runs and the blue triangles 200 particle-MD interaction runs. Taken from Da Costa et al. (2013).

ambient magnetic field $B_0$ again. Its gyrocenter changes again to location O″. By this interaction, the particle gyrocenter has moved from point O to O″.

With the displacement of the proton gyrocenter, the parallel motion of the particle (into or out of the plane of the Figure) will allow the proton to collide with other MDs. We call this time between interactions $\Delta t$. The other MDs will have different cross-sectional radii (a) and different magnetic field intensities ($B_{MD}$). However, if those variables can be taken into account, multiple MD interactions can be accommodated and a diffusion coefficient could be constructed. The usual expression for this cross-field diffusion is $D\perp = (\lambda^2)/\Delta t$, where $\lambda$ is the cross-field displacement.

$$D_\perp = \frac{(M-1)^2}{2aM^2\Delta t}\left[\frac{2a}{3}\left([2M+3]a^2+3M^2r^2\right)+ \right. \\ \left. +\frac{\left(a^2-M^2r^2\right)^2}{\left[M(M-1)\left(a^2-Mr^2\right)\right]^{\frac{1}{2}}}\tanh^{-1}\left(\frac{2a\left[M(M-1)\left(a^2-Mr^2\right)\right]^{\frac{1}{2}}}{(2M-1)a^2-M^2r^2}\right)\right], \quad (1)$$

Equation (1) gives an explicit expression for $D\perp$. In the equation, parameter $M$ is $B_O/B_{MD}$. All of the other parameters are the same as described before. This expression was derived and presented in Tsurutani and Lakhina (2004). The properties of the MDs were determined by measurements of the Ulysses magnetic fields. The statistical values of $a$, $M$, and $\Delta t$ were determined, and then the histograms of each were fitted by functional forms (Tsurutani & Ho, 1999).

The Monte Carlo analysis was performed in the following way. A single proton kinetic energy was selected. The particle pitch angle was assumed to be 45°. This was done so that the particle would have equal parallel and perpendicular speeds. Other angles could be accommodated easily. Each computer run had the proton interact with 100 MDs. Each MD and its properties were determined randomly. This was then performed 1,000 times to get 1,000 values of $\lambda_i$. The 1,000 values of $\lambda_i$ were then used to empirically calculate the cross-field diffusion rates. A detailed description of the analysis can be found in Da Costa et al. (2013).

Figure 25 shows the results of the Da Costa et al. (2013) Monte Carlo analyses. The perpendicular (cross-field) diffusion rate normalized to the Bohm diffusion rate ($D\perp/D_B$) is given as a function of particle energy in MeV. At the left side of the plot, the cross-field diffusion for ~100 keV particles is noted to be ~11% of the Bohm rate. At the far right side of the plots the diffusion rate for ~2 MeV protons is shown to be ~5.5% of the Bohm rate.

It has been noted that in association with the 2012 solar flare that occurred on the far side of the Sun (Baker et al., 2013; Ngwira, Pulkkinen, Kuznetsova, et al., 2013; Ngwira, Pulkkinen, Mays, et al., 2013; Russell et al., 2013), the solar flare energetic ions were detected not only at both STEREO spacecraft but at Earth as well. This indicates that the particles were sensed at ~360° in longitude around the Sun (at a 1 AU distance from the Sun). Although the shocks associated with particle acceleration (Tsurutani, Smith, Pyle, et al., 1982; Tsurutani & Lin, 1985) can extend a good portion of an AU in longitude (at 1 AU), De Lucas (2009) has

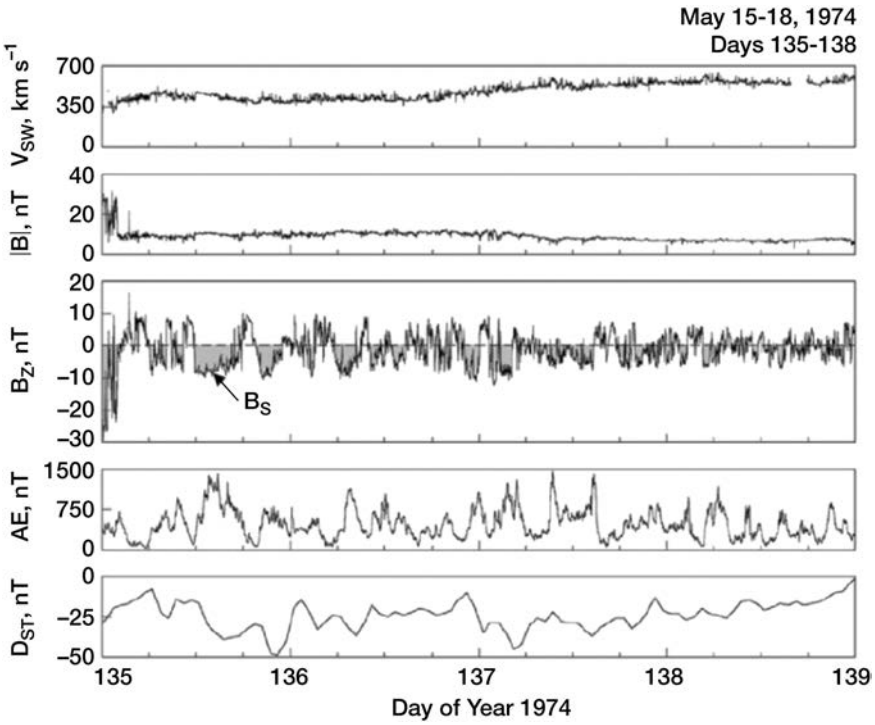


**Figure 26.** Solar wind interplanetary magnetic field $B_Z$ fluctuations (Alfvénic turbulence) and geomagnetic activity (AE and *Dst*). Taken from Tsurutani, Gonzalez, et al. (1995).

indicated that there is only an ~50% chance that interplanetary FSs are detected by two spacecraft separated by ~90° in longitude. Thus, one can assume that shocks do not extend 360° in longitude. Strong cross-field diffusion must be the source of such a broad angular distribution, either near the Sun or in interplanetary space between the Sun and 1 AU. If turbulent "compressions" of the magnetic field such as MDs exist in this region of space, this could possibly account for the energetic particle observations. This could be an interesting area of study for the Solar Orbiter and Solar Probe Plus missions.

### 5.2. Alfvénic Turbulence Effects on Geomagnetic Activity and the Acceleration of Relativistic Magnetospheric Electrons

It has been shown that when the Alfvénic turbulence/waves have southwardly directed magnetic fields just in front of the Earth's magnetosphere, magnetic reconnection occurs (Dungey, 1961) with the Earth's oppositely directed fields (Tsurutani & Gonzalez, 1987). These southwardly directed fields are most likely caused by single wave interactions. The dayside magnetic reconnection leads to nightside reconnection and plasma injections into the midnight sector of the magnetosphere (DeForest & McIlwain, 1971). In HSSs where there is a high level of this Alfvénic turbulence, magnetic reconnection can occur almost continuously for days or even weeks (D'Amicis et al., 2007, 2009, 2010; Gonzalez et al., 2006; Guarnieri, 2006; Hajra et al., 2013; Kozyra et al., 2006; Tsurutani, Gonzalez, et al., 1995; Tsurutani et al., 2006; Tsurutani & Gonzalez, 1987; Turner et al., 2006). These intervals of Alfvénic turbulence and high geomagnetic activity have been called High-Intensity Long-Duration Continuous AE Activity (HILDCAA) intervals. It has been shown by Hajra, Tsurutani, Echer, Gonzalez, Santolik (2015) that such intervals of geomagnetic activity are accompanied by continuous electromagnetic chorus generation. Chorus is believed to lead to relativistic electron acceleration in the magnetosphere (Horne, 2007; Horne & Thorne, 1998; Kasahara et al., 2009; Omura et al., 2015; Summers et al., 1998).

Thus, the generally accepted scenario is that interplanetary Alfvénic turbulence in HSSs leads to magnetic reconnection causing HILDCAAs and midnight sector particle injections. The anisotropic ~10 to 100 keV energetic electrons injected into the magnetosphere cause electromagnetic chorus generation by a temperature anisotropy instability (Kennel & Petschek, 1966). The chorus in turn accelerates the ~100 keV electrons to relativistic energies. Reviews of this idea can be found in Tsurutani et al. (2006, 2010), Kasahara et al. (2009),

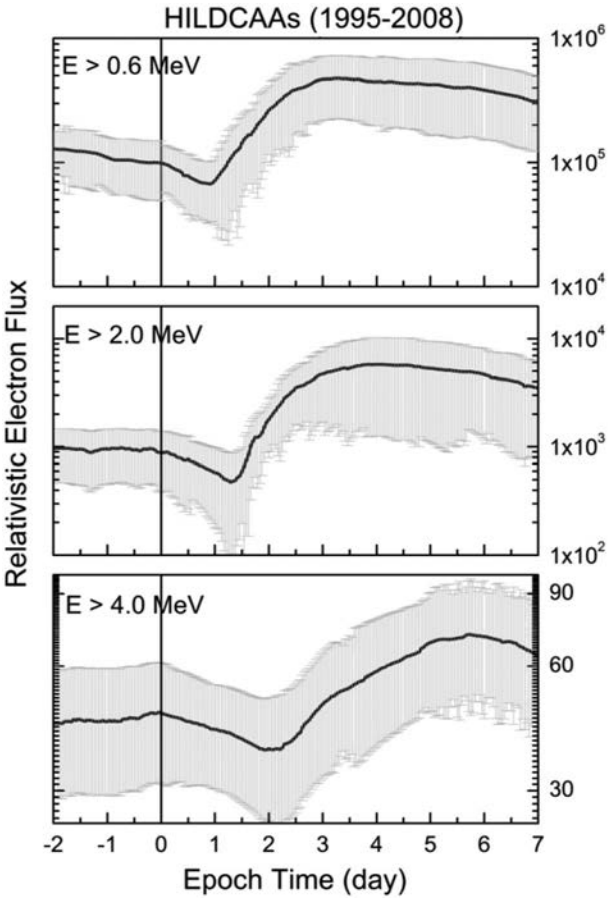


**Figure 27.** Superposed epoch analysis of SC23 High-Intensity Long-Duration Continuous AE Activities and energetic (top) $E > 0.6$ MeV electrons, (middle) $E > 2.0$ MeV electrons, and (bottom) $E > 4.0$ MeV electrons. Taken from Hajra, Tsurutani, Echer, Gonzalez, Santolik (2015).

Miyoshi et al. (2013), and Hajra, Tsurutani, Echer, Gonzalez, Santolik (2015), Hajra, Tsurutani, Echer, Gonzalez, Brum, et al. (2015).

Figure 26 shows an example of solar wind magnetic field fluctuations in $B_z$ and resultant geomagnetic activity at Earth. The panels from the top are the solar wind speed, the magnetic field magnitude, and the IMF $B_z$ component. The bottom two panels are the auroral electrojet index AE and the ring current index, *Dst*. The AE index gives a measure of the intensity of the electrojet current flowing at ~100 km altitude above the auroral zone (~60° to 70° geomagnetic) latitudes. The *Dst* index gives a quantitative estimate of the total energy in the ~10 to 300 keV ions and electrons in the Earth's magnetosphere (Dessler & Parker, 1959; Sckopke, 1966). The satellite used for making the interplanetary measurements was the IMP-8 spacecraft. This is a spacecraft that was in Earth orbit, with an apogee of ~40 $R_E$ and perigee of ~30 $R_E$ (https://directory.eoportal.org/web/eoportal/satellite-missions/i/imp-8). This orbit kept IMP-8 solely in interplanetary space except during short periods when it was in the Earth's geomagnetic tail.

Figure 26 shows that for essentially every major $B_z$ long duration negative excursion (single Alfvén wave cycle), there is a *Dst* decrease. This implies that energetic particles are being injected into the magnetosphere (DeForest & McIlwain, 1971). The responsible processes are midnight sector magnetic reconnection and plasma sheet convection into the magnetosphere. It can also be noted in Figure 26 that for every major $B_z$ negative excursion, there is an AE increase. This implies that energetic charged particles are precipitating into the auroral ionosphere, creating enhanced conductivity in that region.

Figure 27 shows the relationship between HILDCAAs and relativistic electron fluxes in the magnetosphere at $L = 6.6$. All of the HILDCAA events identified in SC23 by Hajra et al. (2013) were used in this superposed epoch analysis. The energetic particle fluxes were obtained from the GOES satellite (Onsager et al., 1996). The zero time in the analyses is the start time of the HILDCAA events. The onset is defined when the AE index first exceeds 200 nT.

The results in Figure 27 show that HILDCAAs precede the occurrence of enhanced relativistic electron fluxes. The $E > 0.6$ MeV electrons appear ~1 day after the onset of HILDCAAs, the $E > 2.0$ MeV fluxes appear ~1.5 days after the HILDCAA onsets, and the $E > 4.0$ MeV fluxes occur ~2 days after the HILDCAA onsets.

The above scenario is in accord with what is expected by the scientific community. HILDCAAs represent substorms and small injection events (Tsurutani et al., 2004). The injection of ~10–100 keV (anisotropic) electrons will cause the generation of electromagnetic whistler mode chorus (Kennel & Petschek, 1966; Meredith et al., 2002; Tsurutani et al., 1979; Tsurutani & Smith, 1977). The chorus will accelerate ~100 keV electrons gradually (Boyd et al., 2014; Horne & Thorne, 1998; Miyoshi et al., 2003). Thus, the ~100 keV electrons will eventually be accelerated to ~0.6 MeV electrons. If the chorus accelerates these ~0.6 MeV energy particles, after some time, the electrons will reach ~2.0 MeV energies, etc. This bootstrap scenario has been proposed in Baker et al. (1994), Li et al. (2005), Turner and Li (2008), and Hajra, Tsurutani, Echer, Gonzalez, and Santolik (2015).

If the interplanetary Alfvén waves are being generated locally (in addition to those generated near the Sun and convected by the solar wind), then certain aspects of the predictability of HILDCAAs and thus predictability of relativistic electrons by upstream monitors might be significantly impaired. Baker et al. (1983) noted that magnetic field measurements made by the ISEE-3 satellite orbiting the L1 libration point only ~0.01 AU upstream of the Earth did not give consistent, particularly good predictability of geomagnetic activity (AE) at Earth. On the contrary, the magnetic field taken by the IMP-8 satellite much closer to the Earth (Figure 26) gives quite excellent correlations between the IMF $B_z$ and AE. The problem might be the growth of new Alfvén waves in the region between the L1 libration point and Earth.

## 6. Final Comments

We have used our past knowledge and analysis techniques of nonlinear phase-steepened cometary plasma waves/turbulence to apply to and study interplanetary Alfvénic waves/turbulence. We have shown that knowing the spectral shape of power spectra is insufficient for understanding the details of the physical processes leading to the formation of plasma turbulence. In particular, waveform and helicity information are extremely important and should be included in any analysis performed. In that aspect, we have used single cycles of cometary plasma waves to decipher the nature of the turbulence and its development. In particular, we have focused on the waveform and helicity (polarization) of the waves.

The example of large-amplitude single-cycle cometary magnetosonic waves (Figure 7) clearly indicates that the wave phase-steepening process leads to a steepened front consisting of a circularly polarized RH (plasma frame) portion followed by a linear compressive portion. The former part of the wave is shortened in time and thus represents high-frequency wave power. The trailing portion is the remainder part of the wave and is low-frequency wave power. The leading portion of the wave contains more than half of the wave phase rotation; thus, the trailing portion contains much less than half of the rotation. We have therefore called the former "wave breaking" and the latter "period doubling." This detailed analysis technique of single wave cycles was then applied to interplanetary HSS Alfvén waves. It was shown that large-amplitude Alfvén waves show very similar features in some sense and very different features in other ways. For large-amplitude Alfvén waves, they were shown to have arc polarization. The wave phase rotation is split ~50–50 in the leading and trailing portions of the wave (different from that of cometary magnetosonic waves). The elongated trailing portion of the wave has nearly doubled its period; thus, we have described this as "period doubling."

It is clear that the evolution of cometary magnetosonic wave turbulence and interplanetary Alfvénic turbulence are very different from each other, although both are plasma wave turbulence detected in the interplanetary medium. The long-lasting wave helicity (polarization) is one obvious feature of difference, but also the splitting of the arc rotation into two parts is another. Thus, the mode of the original waves is perhaps most important to describe the turbulence and its evolution. Helicity may be an enduring feature of the evolutionary process and thus may be a basic characteristic of the turbulence.

In sections 2.7 and 2.8, we again applied the cometary single cycle wave approach to several features of Alfvénic wave turbulence. It was shown that Alfvén waves are often spherical in nature (Figures 16 and 17) and there is evidence of rapid dissipation and evolution (Figure 21). Table 2 shows extremely rapid changes in MDs over ~0.01 AU distance. To replenish the diminished Alfvén wave energy, local generation is needed. Thus, in section 5, we have probed the possibility of local generation of Alfvén waves with the evolution of the high-speed solar wind as the source of energy. Matteini et al. (2006, 2007) and Hellinger and Travnicek (2008) have mentioned the possibility of local Alfvén wave generation though an oblique fire hose instability caused by the expanding solar wind. Another source of free energy for this instability is associated the differential speed between the proton core and beam (or $He^{++}$) distributions (Hellinger & Travnicek, 2011, 2013).

In section 6 we again used the single wave approach. It was shown that single particle interactions with an MD will lead to cross-field displacement of an energetic ion. To identify how many particles will interact with multiple MDs with different characteristics, a Monte Carlo approach was applied. However, the basic physics is the single particle interaction with a single MD.

In section 6 we also examined how components of single cycles of an Alfvén wave train may cause geomagnetic activity and the concomitant acceleration of relativistic electrons in the Earth's magnetosphere.

We have tried to give an informative review of interplanetary turbulence in solar wind HSSs from an observational viewpoint focusing on discontinuities, shocks, MDs, and single Alfvén wave evolution. There are still major unsolved problems that should be mentioned.

Figure 26 shows a strong relationship existing between the IMF $B_z$ components and geomagnetic activity (AE and *Dst*). However, it was noted that the interplanetary measurements were taken by a near-Earth orbiting spacecraft (IMP-8) only ~40 $R_E$ upstream of the Earth. Are observations much further from the Earth useful to predict the onset of HILDCAAs based on solar wind observations? If the predictions are impaired, are they only slightly modified?

Previous attempts have been made to match observations of the IMF at the L1 libration point ~0.01 AU upstream of the Earth to geomagnetic phenomena and indices. This was first done using ISEE-3 observations (Baker et al., 1983) and more recently using ACE data (Guarnieri et al., 2007). Although both spacecraft magnetic field data were excellent for identifying the occurrence of large-scale interplanetary structures such as fast shocks and MCs, they were far less successful in matching the Alfvénic turbulence $B_{south}$ components to the AE index. ISEE-3 had a somewhat "loose" orbit around L1, and it was thought that a tighter orbit would improve matters. The ACE spacecraft was put into this tighter orbit, but still strong correlations like that in Figure 27 have not been found. Thus, at this time, it seems difficult to predict HILDCAAs with a ~30 min advanced warning.

There are days where using ACE interplanetary data gives good correlations to AE and other times when it is less well correlated. Is the local generation of Alfvén waves the cause of lower correlation intervals?

In the body of the text we postponed the discussion of the intermediate and slow shocks until this section of the paper. We have shown that interplanetary Alfvén waves phase-steepen, they are dispersive and dissipative, so are they not intermediate shocks? Diagnoses of the wavefronts are extremely difficult. The presence of the upstream MDs makes analyses of the wavefront normals by standard techniques very difficult, if not impossible. However, from all the ancillary information shown in this paper, intermediate shocks do seem to exist. If these indeed are intermediate shocks, there is a plethora of them, far more than fast shocks.

A similar comment to the above paragraph can be made for the existence of slow shocks. In the body of the text we mentioned that there were too few reported in the literature to consider as a major source of interplanetary turbulence power. Tsurutani and Ho (1999) and Fränz et al. (2000) have determined that most MDs are bounded by sharp magnetic field decreases and sharp magnetic field increases. If these sharp magnetic field magnitude changes are slow shocks as identified for a limited number of cases by Farrugia et al. (2001), then this phenomenon would also be far more common than we currently realize.

What could be the source of Alfvén waves inside 0.3 AU distance from the Sun? Hollweg (2006) discounted granular and supergranular circulation because of a lack of continuity of scale sizes. However, if both of these sources exist, plus further cascading takes place, this idea merits further exploration. Another idea for the generation of low-frequency waves is the solar rotation of nonuniform coronal magnetic fields. This idea was proposed by Hoshino and Takeshima (1993) in application to X-ray binary pulsars and by Glassmeier (1995) applied to Jovian Alfvén waves.

A final related topic should be mentioned. There is the theoretical possibility of the occurrence of rogue plasma waves. This is analogous to large-amplitude rogue ocean waves which have sunk large ships. Can these large-amplitude Alfvénic waves be present in the solar wind as hypothesized by Ruderman (2010), and if so, what effects would they have on the properties of turbulence and geomagnetic activity? Bacha et al. (2017) have hypothesized the existence of ion-acoustic rogue waves in the solar wind associated with a modulational instability. If this is correct, the interplanetary medium at large distances from the Sun may be filled with this phenomenon.

We also expect many surprises to exist in the interplanetary medium close to the Sun. In this article we mentioned several possibilities, "blast wave" shocks and MDs. Those two and many more may await the measurements from the Solar Orbiter, Solar Probe, and Icarus missions.

**Acknowledgments**
Portions of this work were performed at the Jet Propulsion Laboratory, California Institute of Technology, under contract with NASA. G.S.L. thanks the National Academy of Sciences of India for support under the NASI-Platinum Jubilee Senior Scientist Fellowship Scheme. A.S. thanks the Indian National Science Academy (INSA) for their support under the INSA Senior Scientist Fellowship scheme. P.H. acknowledges grant 15-10057S of the Czech Science Foundation. K.H.G. is financially supported by the Deutsches Zentrum für Luft-und Raumfahrt and the Bundesministerium für Wirtschaft und Energie under grants 50OW1203, 50 QW 1101, and 50 OW 1401. The solar wind/interplanetary data at ~1 AU were obtained from the OMNI database (http://omniweb.gsfc.nasa.gov/).The GOES energetic particle data used in this paper were obtained from the website http://www.ngdc.noaa.gov/stp/satellite/goes/dataaccess.html/.The interplanetary data away from Earth orbit and cometary data can be obtained from the NASA Planetary Data System (https://pds.jpl.nasa.gov/).The geomagnetic indices AE, AL, *Dst*, and SYM-H were obtained from the World Data Center for Geomagnetism, Kyoto, Japan (http://wdc.kugi.kyoto-u.ac.jp/). We would like to dedicate this paper to the late Professor Predhiman Krishnan Kaw, who was instrumental for fostering plasma physics not only in India but also the world. A preliminary version of this paper was given as a seminar at the Institute of Plasma Research (IPR), Gandhinagar, India, where Professor Kaw was the founder director.

## References

Abraham-Shrauner, B. (1972). Determination of magnetohydrodynamic shock normal. *Journal of Geophysical Research*, *77*(4), 736–739. https://doi.org/10.1029/JA077i004p00736

Bacha, M., Gougam, L. A., & Tribeche, M. (2017). Ion-acoustic rogue waves in magnetized solar wind plasma with nonextensive electrons. *Physica A*, *466*, 199–210. https://doi.org/10.1016/j.physa.2016.09.013

Baker, D. N., Blake, J. B., Callis, L. B., Cummings, J. R., Hovestadt, D., Kanekal, S., et al. (1994). Relativistic electron acceleration and decay time scales in the inner and outer radiation belts: SAMPEX. *Geophysical Research Letters*, *21*(6), 409–412. https://doi.org/10.1029/93GL03532

Baker, D. N., Li, X., Pulkkinen, A., Ngwira, C. M., Mays, M. L., Galvin, A. B., & Simunac, K. D. C. (2013). A major solar eruptive event in July 2012: Defining extreme space weather scenarios. *Space Weather*, *11*, 585–591. https://doi.org/10.1002/swe.20097

Baker, D. N., Zwickl, R. D., Bame, S. J., Hones, E. W. Jr., Tsurutani, B. T., Smith, E. J., & Akasofu, S.-I. (1983). An ISEE 3 high time resolution study of interplanetary parameter correlations with magnetospheric activity. *Journal of Geophysical Research*, *88*(A8), 6230–6242. https://doi.org/10.1029/JA088iA08p06230

Baumgärtel, K. (1999). Soliton approach to magnetic holes. *Journal of Geophysical Research*, *104*(A12), 28,295–28,308. https://doi.org/10.1029/1999JA900393

Bavassano, B., Dobrowolny, M., & Moreno, G. (1978). Local instabilities of Alfvén waves in high-speed streams. *Solar Physics*, *57*(2), 445–465. https://doi.org/10.1007/BF00160117

Belcher, J. W., & Davis, J. L. (1971). Large-amplitude Alfvén waves in the interplanetary medium, 2. *Journal of Geophysical Research*, *76*(16), 3534–3563. https://doi.org/10.1029/JA076i016p03534

Belcher, J. W., & Solodyna, C. V. (1975). Alfvén waves and directional discontinuities in the interplanetary medium. *Journal of Geophysical Research*, *80*(1), 181–186. https://doi.org/10.1029/JA080i001p00181

Boyd, A. J., Spence, H. E., Claudepierre, S. G., Fennell, J. F., Blake, J. B., Baker, D. N., et al. (2014). Quantifying the radiation belt seed population in the March 17, 2013 electron acceleration event. *Geophysical Research Letters*, *41*, 2275–2281. https://doi.org/10.1002/2014GL050626

Brinca, A. L. (1991). Cometary linear instabilities: From profusion to prospective. In A. Johnstone (Ed.), *Cometary plasma processes* (Vol. 61, pp. 211–221). Washington, DC: AGU Press.

Bruno, R., & Carbone, V. (2013). The solar wind as a turbulence laboratory. *Living Reviews in Solar Physics*, *10*(2). https://doi.org/10.12942/lrsp-2013-2

Burlaga, L. F. (1971). Nature and origin of directional discontinuities in the solar wind. *Journal of Geophysical Research*, *76*(19), 4360–4365. https://doi.org/10.1029/JA076i019p04360

Burlaga, L. F., & Chao, J. K. (1971). Reverse and forward slow shocks in the solar wind. *Journal of Geophysical Research*, *76*, 7516.

Burlaga, L. F., Lemaire, J. F., & Turner, J. M. (1977). Interplanetary current sheets at 1 AU. *Journal of Geophysical Research*, *82*(22), 3191–3200. https://doi.org/10.1029/JA082i022p03191

Burlaga, L. F., Sittler, E., Mariani, F., & Schwenn, R. (1981). Magnetic loop behind an interplanetary shock: Voyager, Helios and IMP-8 observations. *Journal of Geophysical Research*, *86*(A8), 6673. https://doi.org/10.1029/JA086iA08p06673

Buti, B., Jayanti, V., Vinas, A. F., Ghosh, S., Goldstein, M. L., Roberts, D. A., et al. (1998). Nonlinear evolution of Alfvén wave packets. *Geophysical Research Letters*, *25*(13), 2377–2380. https://doi.org/10.1029/98GL01688

Buti, B., Tsurutani, B. T., Neugebauer, M., & Goldstein, B. E. (2001). Generation mechanism for magnetic holes in the solar wind. *Geophysical Research Letters*, *28*(7), 1355–1358. https://doi.org/10.1029/2000GL012592

Chao, J. K., & Olbert, S. (1970). Observation of slow shocks in interplanetary space. *Journal of Geophysical Research*, *75*(31), 6394–6397. https://doi.org/10.1029/JA075i031p06394

Chen, C. H. K., Sorriso-Valvo, L., Safrankova, J., & Nemecek, Z. (2014). Intermittency of solar wind density fluctuations from ion to electron scales. *Astrophysical Journal Letters*, *789*(L8), 5. https://doi.org/10.1088/2041-8205/789/1/L8

Chew, G. F., Goldberger, M. L., & Low, F. E. (1956). The Boltzmann equation and the one-fluid hydromagnetic equations in the absence of particle collisions. *Proceedings. Royal Society of London*, *236*(1204), 112–118. https://doi.org/10.1098/rspa.1956.0116

Colburn, D. S., & Sonett, C. P. (1966). Discontinuities in the solar wind. *Space Science Reviews*, *5*, 439.

Coleman, P. J. (1968). Turbulence, viscosity and dissipation in the solar wind plasma. *The Astrophysical Journal*, *153*, 371. https://doi.org/10.1086/149674

Da Costa, E. Jr., Tsurutani, B. T., Alves, M. V., Echer, E., & Lakhina, G. S. (2013). Cross-field diffusion of energetic (100 keV to 2 MeV) protons in interplanetary space. *The Astrophysical Journal*, *778*(2), 180. https://doi.org/10.1088/0004-637X/778/2/180

D'Amicis, R., Bruno, R., & Bavassano, B. (2007). Is geomagnetic activity driven by solar wind turbulence? *Geophysical Research Letters*, *34*, L05108. https://doi.org/10.1029/2006GL028896

D'Amicis, R., Bruno, R., & Bavassano, B. (2009). Alfvénic turbulence in high speed solar wind streams as a driver for auroral activity. *Journal of Atmospheric and Solar - Terrestrial Physics*, *71*(10-11), 1014–1022. https://doi.org/10.1016/j.jastp.2008.05.002

D'Amicis, R., Bruno, R., & Bavassano, B. (2010). Geomagnetic activity driven by solar wind turbulence. *Advances in Space Research*, *46*(4), 514–520. https://doi.org/10.1016/j.asr.2009.08.031

Dasgupta, B., Tsurutani, B. T., & Janaki, M. S. (2003). A kinetic approach to the ponderomotive force. *Geophysical Research Letters*, *30*(21), 2128. https://doi.org/10.1029/2003GL017385

De Lucas, A. (2009). A study of shock wave fronts and magnetic cloud's extent (PhD thesis, INPE-13269-MAN/45).

DeForest, S. E., & McIlwain, C. E. (1971). Plasma clouds in the magnetosphere. *Journal of Geophysical Research*, *76*(16), 3587–3611. https://doi.org/10.1029/JA076i016p03587

Delaboudinière, J.-P., Artzner, G. E., Gabriel, A. H., Hochedez, J. F., et al. (1995). EIT: Extreme-Ultraviolet Imaging Telescope for the SOHO mission. *Solar Physics*, *162*(1-2), 291–312. https://doi.org/10.1007/BF00733432

Dessler, A. J., & Parker, E. N. (1959). Hydromagnetic theory of magnetic storms. *Journal of Geophysical Research*, *64*(12), 2239–2252. https://doi.org/10.1029/JZ064i012p02239

Dobrowolny, M. (1972). Kelvin-Helmholtz instability in a high β collisionless plasma. *Physics of Fluids*, *15*(12), 2263. https://doi.org/10.1063/1.1693866

Dobrowolny, M. (1977). Velocity shear instability of Alfvén waves in a high β collisionless plasma. *Physics of Fluids*, *20*(6), 1027. https://doi.org/10.1063/1.861972

Dungey, J. W. (1961). Interplanetary magnetic field and the auroral zones. *Physical Review Letters*, *6*(2), 47–48. https://doi.org/10.1103/PhysRevLett.6.47

Echer, E., Gonzalez, W. D., Tsurutani, B. T., & Gonzalez, A. L. C. (2008). Interplanetary conditions causing intense geomagnetic storms (Dst $\leq -100$ nT) during solar cycle 23 (1996–2006). *Journal of Geophysical Research*, *113*, A05221. https://doi.org/10.1029/2007JA012744

Echer, E., Tsurutani, B. T., & Guarnieri, F. L. (2010). Forward and reverse CIR shocks at 4–5 AU: Ulysses. *Advances in Space Research*, *45*(6), 798–803. https://doi.org/10.1016/j.asr.2009.11.011

Echer, E., Tsurutani, B. T., Guarnieri, F. L., & Kozyra, J. U. (2011). Interplanetary fast forward shocks and their geomagnetic effects: CAWSES events. *Journal of Atmospheric and Solar - Terrestrial Physics*, *73*(11-12), 1330–1338. https://doi.org/10.1016/j.jastp.2010.09.020

Elsasser, W. M. (1950). The hydromagnetic equations. *Physiological Research*, *79*(1), 183. https://doi.org/10.1103/PhysRev.79.183

Farrugia, C. J., Vasquez, B., Richardson, I. G., Torbert, R. B., Burlaga, L. F., Biernat, H. K., et al. (2001). A reconnection layer associated with a magnetic cloud. *Advances in Space Research*, *28*(5), 759–764. https://doi.org/10.1016/S0273-1177(01)00529-4

Forsyth, R. J., Balogh, A., Horbury, T. S., Erdos, G., Smith, E. J., & Burton, M. E. (1996). The heliospheric magnetic field at solar minimum: Ulysses observations from pole to pole. *Astronomy and Astrophysics*, *316*, 287–295.

Fox, N. J., Velli, M. C., Bale, S. D., Decker, R., Driesman, A., Howard, R. A., et al. (2015). The Solar Probe Plus mission: Humanity's first visit to our star. *Space Science Reviews*, *204*(1-4), 7–48.

Fränz, M., Burgess, D., & Horbury, T. S. (2000). Magnetic depressions in the solar wind. *Journal of Geophysical Research*, *105*(A6), 12,725–12,732. https://doi.org/10.1029/2000JA900026

Frisch, U. (1995). *Turbulence*. Cambridge, UK: Cambridge University Press.

Gary, S. P., McKean, M. E., & Winske, D. (1993). Ion anisotropy instabilities in the magnetosheath: Theory and simulations. *Journal of Geophysical Research*, *98*(A3), 3963–3971. https://doi.org/10.1029/92JA02585

Genot, V., Budnik, E., Hellinger, P., Passot, T., Belmont, G., Travnicek, P. M., et al. (2009). Mirror structures above and below the linear instability threshold: Cluster observations, fluid model and hybrid simulations. *Annales Geophysicae*, *27*(2), 601–615. https://doi.org/10.5194/angeo-27-601-2009

Glassmeier, K.-H. (1995). Ultralow frequency pulsations, Earth and Jupiter compared. *Advances in Space Research*, *16*(4), 209–218.

Glassmeier, K.-H. (2017). Interaction of the solar wind with comets: A Rosetta perspective. *Philosophical Transactions of the Royal Society A*, *375*(2097). https://doi.org/10.1098/rsta.2016.02

Glassmeier, K.-H., Coates, A. J., Acuña, M. H., Goldstein, M. L., Johnstone, A. D., Neubauer, F. M., & Rème, H. (1989). Spectral characteristics of low-frequency plasma turbulence upstream of comet P/Halley. *Journal of Geophysical Research*, *94*(A1), 37–48. https://doi.org/10.1029/JA094iA01p00037

Glassmeier, K.-H., & Neubauer, F. M. (1993). Low-frequency electromagnetic plasma waves at comet P/Grigg-Skjellerup: Overview and spectral characteristics. *Journal of Geophysical Research*, *98*(A12), 20,921–20,935. https://doi.org/10.1029/93JA02583

Glassmeier, K.-H., Neubauer, F. M., Acuña, M. H., & Mariani, F. (1987). Low frequency magnetic field fluctuations in comet P/Halley magnetosheath: Giotto observations. *Astronomy and Astrophysics*, *187*, 65.

Goetz, C., Koenders, C., Hansen, K. C., Burch, J., Carr, C., Eriksson, A., et al. (2016). Structure and evolution of the diamagnetic cavity at Comet 67P/Churyumov-Gerasimenko. *Monthly Notices of the Royal Astronomical Society*, *462*, S459–S467.

Goetz, C., Koenders, C., Richter, I., Altwegg, K., Burch, J., Carr, C., et al. (2016). First detection of a diamagnetic cavity at comet 67P/Churyumov-Gerasimenko. Astronomy and Astrophysics. *Astronomy and Astrophysics*, *588*, A24. https://doi.org/10.1051/0004-6361/201527728

Gold, T. (1955). Magnetic storms. In *Gas dynamics of cosmic clouds* (103 pp.). Amsterdam: North Holland.

Goldstein, B. E., Neugebauer, M., Zhang, L. D., & Gary, S. P. (2000). Observed constraint on proton-proton relative velocities in the solar wind. *Geophysical Research Letters*, *27*(1), 53–56. https://doi.org/10.1029/1999GL003637

Gonzalez, W. D., Guarnieri, F. L., Clua-Gonzalez, A. L., Echer, E., Alves, M. V., Ogino, T., & Tsurutani, B. T. (2006). Magnetospheric energetics during HILDCAAs. In B. T. Tsurutani, et al. (Eds.), *Recurrent magnetic storms: Corotating solar wind streams* (Vol. 167, pp. 175–182). Washington, DC: AGU Press.

Gonzalez, W. D., Joselyn, J. A., Kamide, Y., Kroehl, H. W., Rostoker, G., Tsurutani, B. T., & Vasyliunas, V. M. (1994). What is a geomagnetic storm? *Journal of Geophysical Research*, *99*(A4), 5571–5792.

Guarnieri, F. L. (2006). The nature of auroras during High-Intensity Long-Duration Continuous AE Activity (HILDCAA) events: 1998–2001. In B. T. Tsurutani, et al. (Eds.), *Recurrent magnetic storms: Corotating solar wind streams* (Vol. 167, pp. 235–243). Washington, DC: AGU Press.

Guarnieri, F. L., Tsurutani, B. T., Echer, E., & Gonzalez, W. D. (2007). In M. Duldig, et al. (Eds.), *Geomagnetic activity and auroras caused by high-speed streams: A review*, *Adv. Geosci., 8, Sol. Terr.*, Hackensack, NJ: World Scientific.

Hajra, R., Echer, E., Tsurutani, B. T., & Gonzalez, W. D. (2013). Solar cycle dependence of High-Intensity Long-Duration Continuous AE Activity (HILDCAA) events, relativistic electron predictors? *Journal of Geophysical Research: Space Physics*, *118*, 5626–5638. https://doi.org/10.1002/jgra.50530

Hajra, R., Echer, E., Tsurutani, B. T., & Gonzalez, W. D. (2014). Solar wind-magnetosphere energy coupling efficiency and partitioning: HILDCAAs and preceding CIR storms during solar cycle 23. *Journal of Geophysical Research: Space Physics*, *119*, 2675–2690. https://doi.org/10.1002/2013JA019646

Hajra, R., Tsurutani, B. T., Echer, E., Gonzalez, W. D., Brum, C. G., Viera, L. E. A., & Santolik, O. (2015). Relativistic electron acceleration during HILDCAA events: Are precursor CIR magnetic storms important? *Earth, Planets and Space*, *67*(1), 109. https://doi.org/10.1186/s40623-015-0280.5

Hajra, R., Tsurutani, B. T., Echer, E., Gonzalez, W. D., & Santolik, O. (2015). Relativistic ($E > 0.6$, $>2.0$ and $>4.0$ MeV) electron acceleration at geosynchronous orbit during high-intensity, long-duration, continuous AE activity (HILDCAA) events. *The Astrophysical Journal*, *799*(1). https://doi.org/10.1088/0004-637X/799/1/39

Hasegawa, A. (1969). Drift mirror instability in the magnetosphere. *Physics of Fluids*, *12*(12), 2642. https://doi.org/10.1063/1.1692407

Hasegawa, A., & Tsurutani, B. T. (2011). Mirror mode expansion in planetary magnetosheaths: Bohm-like diffusion. *Physical Review Letters*, *107*(24), 245,005. https://doi.org/10.1103/PhysRevLett.107.245005

Hellinger, P. (2007). Comment on the linear mirror instability near the threshold. *Physics of Plasmas*, *14*(8), 082105. https://doi.org/10.1063/1.2768318

Hellinger, P., Landi, S., Matteini, L., Verdini, A., & Franci, L. (2017). Mirror instability in the turbulent solar wind. *The Astrophysical Journal*, *838*(2), 158. https://doi.org/10.3847/1538-4357/aa67e0

Hellinger, P., & Travnicek, P. M. (2008). Oblique proton fire hose instability in the expanding solar wind: Hybrid simulations. *Journal of Geophysical Research*, *113*, A10109. https://doi.org/10.1029/2008JA013416

Hellinger, P., & Travnicek, P. M. (2011). Proton core-beam system in the expanding solar wind: Hybrid simulations. *Journal of Geophysical Research*, *116*, A11101. https://doi.org/10.1029/2011JA016940

Hellinger, P., & Travnicek, P. M. (2013). Protons and alpha particles in the expanding solar wind: Hybrid simulations. *Journal of Geophysical Research: Space Physics*, *118*, 5421–5430. https://doi.org/10.1002/jgra.50540

Hellinger, P., Travnicek, P. M., Stverak, S., Matteini, L., & Velli, M. (2013). Proton thermal energetics in the solar wind: Helios reloaded. *Journal of Geophysical Research: Space Physics*, *118*, 1351–1365. https://doi.org/10.1002/jgra.50107

Ho, C. M., Tsurutani, B. T., Smith, E. J., & Feldman, W. C. (1994). A detailed examination of an X-line region in the distant tail: ISEE-3 observations of jet flow and Bz reversals and a pair of slow shocks. *Geophysical Research Letters*, *21*(25), 3031–3034. https://doi.org/10.1029/94GL02096

Hollweg, J. V. (2006). The solar wind: Then and now. In *Rcurrent magnetic storms: Corotating solar wind streams* (Vol. 167, pp. 19–27). Washington, DC: AGU Press.

Horbury, T., Burgess, D., & Fränz, M. (2001). Three spacecraft observations of solar wind discontinuities. *Geophysical Research Letters*, *28*, 677.

Horbury, T., & Tsurutani, B. (2001). Ulysses measurements of waves, turbulence and discontinuities. In A. Balogh, et al. (Eds.), *The heliosphere near solar minimum, the Ulysses perspective* (pp. 167–227). UK: Springer.

Horne, R. B. (2007). Acceleration of killer electrons. *Nature Physics*, *3*(9), 590–591. https://doi.org/10.1038/nphys703

Horne, R. B., & Thorne, R. M. (1998). Potential waves for relativistic electron scattering and stochastic acceleration during magnetic storms. *Geophysical Research Letters*, *25*(15), 3011–3014. https://doi.org/10.1029/98GL01002

Hoshino, M., & Takeshima, T. (1993). A turbulent model of time variability in X-ray binary pulsars. *The Astrophysical Journal*, *411*, L79. https://doi.org/10.1086/186917

Hsieh, W.-C., Shue, J.-H., Chao, J.-K., Tsai, T.-C., Nemecek, Z., & Safrankova, J. (2014). Possible observational evidence of contact discontinuities. *Geophysical Research Letters*, *41*, 8228–8234. https://doi.org/10.1002/2014GL062342

Hundhausen, A. J. (1985). Some macroscopic properties of shock waves in the heliosphere. In R. G. Stone & B. T. Tsurutani (Eds.), *Collisionless shocks in the heliosphere: A tutorial review*, *AGU Monograph* (Vol. 34, pp. 37–58). Washington, DC: AGU Press.

Iyemori, T. (1990). Storm-time magnetospheric currents inferred from mid-latitude geomagnetic field variations. *Journal of Geomagnetism and Geoelectricity*, *42*, 1249. https://doi.org/10.5636/jgg.42.1249
Jeffrey, A., & Taniuti, T. (1964). *Non-linear wave propagation*. New Yok, NY: Academic Press.
Jones, G. H., & Balogh, A. (2003). The global heliospheric magnetic field polarity distribution as seen at Ulysses. *Annales Geophysicae*, *21*(6), 1377–1382. https://doi.org/10.5194/angeo-21-1377-2003
Kantrowitz, A., & Petschek, H. E. (1966). MHD characteristics and shock waves. In W. B. Kunkel (Ed.), *Plasma physics in theory and application*, (chap. 5, pp. 148–207). New York: McGraw Hill.
Kasahara, Y., Miyoshi, Y., Omura, Y., Verkhoglyadova, O. P., Nagano, I., Kimura, I., & Tsurutani, B. T. (2009). Simultaneous satellite observations of VLF chorus, hot and relativistic electrons in a magnetic storm "recovery" phase. *Geophysical Research Letters*, *36*, L01106. https://doi.org/10.1029/2008GL036454
Kennel, C. F., Edmiston, J. P., & Hada, T. (1985). A quarter century of collisionless shock research. In R. G. Stone & B. T. Tsurutani (Eds.), *Collisionless shocks in the heliosphere: A tutorial review*, *AGU Monograph* (Vol. 34, pp. 1–36). Washington, DC: AGU Press.
Kennel, C. F., & Petschek, H. E. (1966). Limit of stably trapped particle fluxes. *Journal of Geophysical Research*, *71*(1), 1–28. https://doi.org/10.1029/JZ071i001p00001
Khazanov, G. V., Moore, T. E., Krivorutsky, E. N., Horwitz, J. L., & Liemohn, M. W. (1996). Lower hybrid turbulence and ponderomotive force effects in space plasmas subjected to large-amplitude low-frequency waves. *Geophysical Research Letters*, *23*(8), 797–800. https://doi.org/10.1029/96GL00844
Klein, L. W., & Burlaga, L. F. (1982). Interplanetary magnetic clouds at 1 AU. *Journal of Geophysical Research*, *87*(A2), 613. https://doi.org/10.1029/JA087iA02p00613
Knetter, T., Neubauer, F. M., Horbury, T., & Balogh, A. (2004). Four-point discontinuity observations using Cluster magnetic field data: A statistical survey. *Journal of Geophysical Research*, *109*(A6), 6102. https://doi.org/10.1029/2003JA010099
Kozyra, J. U., Crowley, G., Emery, B. A., et al. (2006). Response of the upper/middle atmosphere to coronal holes and powerful high-speed solar wind streams. In B. T. Tsurutani, et al. (Eds.), *Recurrent magnetic storms: Corotating solar wind streams* (Vol. 167, pp. 319–340). Washington, DC: AGU Press.
Kraichnan, R. H. (1965). Inertial-range spectrum of hydromagnetic turbulence. *Physics of Fluids*, *8*(7), 1385–1387. https://doi.org/10.1063/1.1761412
Krasnosselskikh, V., et al. (2016). ICARUS: Investigation of coronal acceleration and heating up to the Sun, Mission Proposal Submitted to the European Space Agency (ESA), LPC2E/CNRS, University Orleans, France.
Krieger, A. S., Timothy, A. F., & Roelof, E. C. (1973). A coronal hole and its identification as the source of a high velocity solar wind stream. *Solar Physics*, *23*, 123.
Lakhina, G. S. (1987). Low frequency electrostatic noise due to velocity shear instabilities in the regions of magnetospheric flow boundaries. *Journal of Geophysical Research*, *92*(A11), 12,161–12,170. https://doi.org/10.1029/JA092iA11p12161
Lakhina, G. S. (1990). Generation of ULF waves in the polar cusp region by velocity shear-driven kinetic Alfvén modes. *Astrophysics and Space Science*, *165*(1), 153–161. https://doi.org/10.1007/BF00653667
Lakhina, G. S., Tsurutani, B. T., & Pickett, J. S. (2004). Association of Alfvén waves and proton cyclotron waves with electrostatic bipolar pulses: Magnetic hole events observed by Polar. *Nonlinear Processes in Geophysics*, *11*(2), 205–213. https://doi.org/10.5194/npg-11-205-2004
Landau, L. D., & Lifschitz, E. M. (1960). *Electrodynamics of continuous media* (p. 255). New York: Pergamon Press.
Lazarian, A., Vlahos, L., Kowal, G., Yan, H., Beresnyak, A., & de Gouveia Dal Pino, E. M. (2012). Turbulence, magnetic reconnection in turbulent fluids and energetic particle acceleration. *Space Science Reviews*, *173*(1-4), 557–622. https://doi.org/10.1007/s11214-012-9936-7
Le Roux, J. A., Zank, G. P., Webb, G. M., & Khabarova, O. (2015). A kinetic transport theory for particle acceleration and transport in regions of multiple contracting and reconnecting inertial-scale flux ropes. *The Astrophysical Journal*, *801*(2), 112. https://doi.org/10.1088/0004-637X/801/2/112
Lepping, R. P., & Behannon, K. W. (1980). Magnetic field directional discontinuities: 1. Minimum variance errors. *Journal of Geophysical Research*, *85*, 4695.
Lepping, R. P., & Behannon, K. W. (1986). Magnetic field directional discontinuities: Characteristics between 0.46 and 1.0 AU. *Journal of Geophysical Research*, *91*, 8725.
Levy, R. H., Petschek, H. E., & Siscoe, G. L. (1964). Aerodynamic aspects of the magnetospheric flow. *AIAA Journal*, *2*(12), 2065–2076. https://doi.org/10.2514/3.2745
Li, X., Baker, D. N., Temerin, M., Reeves, G. D., Friedel, R., & Shen, C. (2005). Energetic electrons, 50 keV to 6 MeV, at geosynchronous orbit: Their responses to solar wind variations. *Space Weather*, *3*, S04001. https://doi.org/10.1029/2004SW000105
Lin, N., Kellogg, P. J., MacDowall, R. J., Balogh, A., Forsyth, R. J., Phillips, J. L., et al. (1995). Observations of plasma waves in magnetic holes. *Geophysical Research Letters*, *22*, 2417–3420.
Lin, N., Kellogg, P. J., MacDowall, R. J., Tsurutani, B. T., & Ho, C. M. (1996). Langmuir waves associated with discontinuities in the solar wind: A statistical study. *Astronomy and Astrophysics*, *316*, 425–429.
Lugaz, N., Farrugia, C. J., Winslow, R. M., Al-Haddad, N., Kilpua, E. K. J., & Riley, P. (2016). Factors affecting the geoeffectiveness of shocks and sheaths at 1 AU. *Journal of Geophysical Research: Space Physics*, *121*, 10,861–10,879. https://doi.org/10.1002/2016JA023100
MacDowall, R. J., Lin, N., Kellogg, P. J., Balogh, A., Forsyth, R. J., & Neugebauer, M. (1996). Langmuir waves in magnetic holes: Source mechanism and consequences. In D. Winterhalter, et al. (Eds.), *Proc. Eighth Intl. Sol. Wind Conf., Am. Inst. Phys.* (Vol. 382, pp. 301–304).
Marsch, E., & Livi, S. (1987). Observational evidence for marginal stability of solar wind ion beams. *Journal of Geophysical Research*, *92*, 7263–7268.
Marsch, E., & Mangeney, A. (1987). Ideal MHD equations in terms of compressive Elsässer variables. *Journal of Geophysical Research*, *92*(A7), 7363–7367. https://doi.org/10.1029/JA092iA07p07363
Marsch, E., Marsden, R., Harrison, R., Wimmer-Schweingruber, R., & Fleck, B. (2005). Solar Orbiter—mission profile, main goals and present status. *Advances in Space Research*, *36*(8), 1360–1366. https://doi.org/10.1016/j.asr.2004.11.012
Marsch, E., Mülhäuser, K. H., Schwenn, R., Rosenbauer, H., Pilipp, W., & Neubauer, F. M. (1982). Solar wind protons: Three-dimensional velocity distributions and derived plasma parameters measured between 0.3 and 1 AU. *Journal of Geophysical Research*, *87*(A1), 52–72.
Matteini, L., Hellinger, P., Goldstein, B. E., Landi, S., Velli, M., & Neugebauer, M. (2013). Signatures of kinetic instabilities in the solar wind. *Journal of Geophysical Research: Space Physics*, *118*, 2771–2782. https://doi.org/10.1002/jgra.50320
Matteini, L., Hellinger, P., Landi, S., Travnicek, P. M., & Velli, M. (2012). Ion kinetics in the solar wind: Coupling global expansion to local microphysics. *Space Science Reviews*, *172*(1-4), 373–396. https://doi.org/10.1007/s11214-011-9774-z
Matteini, L., Horbury, T. S., Pantellini, F., Velli, M., & Schwartz, S. J. (2015). Ion kinetic energy conservation and magnetic field strength constancy in multi-fluid solar wind Alfvénic turbulence. *The Astrophysical Journal*, *802*(1), 11. https://doi.org/10.1088/0004-637X/802/1/11

Matteini, L., Landi, S., Hellinger, P., Pantellini, F. G., Maksimovic, M., Velli, M., et al. (2007). The evolution of the solar wind proton temperature anisotropy from 0.3 to 2.5 AU. *Geophysical Research Letters*, *34*, L20105. https://doi.org/10.1029/2007GL030920

Matteini, L., Landi, S., Hellinger, P., & Velli, M. (2006). Parallel proton fire hose instability in the expanding solar wind: Hybrid simulations. *Journal of Geophysical Research*, *111*, A10101. https://doi.org/10.1029/2006JA011667

Matthaeus, W. H., & Velli, M. (2011). Who needs turbulence? A review of turbulence effects in the heliosphere and on the fundamental process of reconnection. *Space Science Reviews*, *160*(1-4), 145–168. https://doi.org/10.1007/s11214-011-9793-9

Matthaeus, W. H., Wan, M., Servidio, S., Greco, A., Osman, K. T., Oughton, S., & Dmitruk, P. (2015). Intermittency, nonlinear dynamics and dissipation in the solar wind and astrophysical plasmas. *Philosophical Transactions of the Royal Society A*, *373*(2041). https://doi.org/10.1098/rsta.2014.0154

McComas, D. J., Elliott, H. A., Gosling, J. T., Reisenfeld, D. B., Skoug, R. M., Goldstein, B. E., et al. (2002). Ulysses second fast latitude scan; complexity near solar maximum and the reformation of polar coronal holes. *Geophysical Research Letters*, *29*(9), 1290. https://doi.org/10.1029/2001GL014164

Meredith, N. P., Horne, R. B., Iles, R. H. A., Thorne, R. M., Heynderickx, D., & Anderson, R. R. (2002). Outer zone relativistic electrons associated with substorm-enhanced whistler mode chorus. *Journal of Geophysical Research*, *107*(A7), 1144. https://doi.org/10.1029/2001JA9009700

Miyoshi, Y., Kataoka, R., Kasahara, H., Kumamoto, A., Nagai, T., & Thomsen, M. F. (2013). High-speed solar wind with southward interplanetary magnetic field causes relativistic electron flux enhancement of the outer radiation belt via enhanced condition of whistler waves. *Geophysical Research Letters*, *40*, 4520–4525. https://doi.org/10.1002/grl.50916

Miyoshi, Y., Morioka, A., Obara, T., Misawa, H., Nagai, T., & Kasahara, Y. (2003). Rebuilding process of the outer radiation belt during the November 1993 magnetic storm: NOAA and Exos-D observations. *Journal of Geophysical Research*, *108*(A1), 1004. https://doi.org/10.1029/2001JA007542

Montgomery, D., & Turner, L. (1981). Anisotropic magnetohydrodynamic turbulence in a strong external magnetic field. *Physics of Fluids*, *24*(5), 825–831. https://doi.org/10.1063/1.863455

Nerney, S. F., & Suess, S. T. (2005). Stagnation flow in the thin streamer boundaries. *The Astrophysical Journal*, *624*(1), 378–391. https://doi.org/10.1086/428924

Ness, N. F., Scearce, C. S., & Seek, J. B. (1964). Initial results of the IMP 1 magnetic field experiment. *Journal of Geophysical Research*, *69*(17), 3531–3569. https://doi.org/10.1029/JZ069i017p03531

Neubauer, F. M., Glassmeier, K.-H., Pohl, M., Roeder, J., Acuna, M. H., Burlaga, L. F., et al. (1986). First results from the Giotto magnetometer instrument at comet Halley. *Nature*, *321*(6067), 352–355. https://doi.org/10.1038/321352a0

Neugebauer, M. (2006). Comment on the abundances of rotational and tangential discontinuities in the solar wind. *Journal of Geophysical Research*, *111*, A04103. https://doi.org/10.1029/2005JA011497

Neugebaueer, M., & Giacalone, J. (2010). Progress in the study of interplanetary discontinuities. *American Institute of Physics*, *1216*, 194–199. https://doi.org/10.1063/1.3395834

Neugebauer, M., Clay, D. R., Goldstein, B. E., Tsurutani, B. T., & Zwickl, R. D. (1984). A reexamination of rotational and tangential discontinuities in the solar wind. *Journal of Geophysical Research*, *89*(A7), 5395–5648. https://doi.org/10.1029/JA089iA07p05395

Neugebauer, M., Goldstein, B. E., Winterhalter, D., Smith, E. J., MacDowall, R. J., & Gary, S. P. (2001). Ion distributions in large magnetic holes in the fast solar wind. *Journal of Geophysical Research*, *106*(A4), 5635–5648. https://doi.org/10.1029/2000JA000331

Neupert, W. M., & Pizzo, V. (1974). Solar coronal holes as sources of recurrent geomagnetic disturbances. *Journal of Geophysical Research*, *79*(25), 3701–3709. https://doi.org/10.1029/JA079i025p03701

Ngwira, C. M., Pulkkinen, A., Kuznetsova, M. M., & Glocer, A. (2013). Modeling extreme Carrington-type space weather events using three-dimensional global MHD simulations. *Journal of Geophysical Research*, *119*, 4456–4474. https://doi.org/10.1002/2013JA0199661

Ngwira, C. M., Pulkkinen, A., Mays, M. L., Kuznetsova, M. M., Galvin, A. B., et al. (2013). Simulation of the 23 July 2012 extreme space weather event: What if this extremely rare CME was Earth directed? *Space Weather*, *11*, 671–679. https://doi.org/10.1002/2013SW000990

Oliveira, D. M., & Raeder, J. (2015). Impact angle control of interplanetary shock geoeffectiveness. *Journal of Geophysical Research*, *119*, 8188–8201. https://doi.org/10.1002/2014JA020275

Omura, Y., Miyashita, Y., Yoshikawa, M., Summers, D., Hikishima, M., Ebihara, Y., & Kubota, Y. (2015). Formation processes of relativistic electron flux through interaction with chorus emissions in the Earth's inner magnetosphere. *Journal of Geophysical Research: Space Physics*, *120*, 9545–9562. https://doi.org/10.1002/2015JA021563

Onsager, T. G., Grubb, R., Kunches, J., Matheson, L., Speich, D., Zwickl, R., & Sauer, H. (1996). Operational uses of the GOES energetic particle detectors. *Proceedings of SPIE*, *2812*, 281–290.

Papadopoulos, K. (1985). Microinstabilities and anomalous transport. In R. G. Stone & B. T. Tsurutani (Eds.), *Collisionless shocks in the heliosphere: A tutorial review* (Vol. 34, pp. 59–90). Washington, DC: American Geophysical Union.

Phillips, J. L., Balogh, A., Bame, S. J., Goldstein, B. E., Gosling, J. T., Hoeksema, H. T., et al. (1994). Ulysses at 50 south: Constant immersion in the high-speed solar wind. *Geophysical Research Letters*, *21*(12), 1105–1108. https://doi.org/10.1029/94GL01065

Pizzo, V. J. (1985). Interplanetary shocks on the large scale: A retrospective on the last decade's theoretical efforts. In *Collisionless shocks in the heliosphere, reviews of current research*, R. G. Stone & B. T. Tsurutani (Eds.), *Geophysical Monograph Series* (Vol. 35, pp. 51–68). Washington, DC: American Geophysical Union.

Pokhotelov, O. A., Sagdeev, R. Z., Balikhin, M. A., Onischenko, O. G., & Fedun, V. N. (2008). Nonlinear mirror waves in non-Maxwellian space plasmas. *Journal of Geophysical Research*, *113*, 02445. https://doi.org/10.1029/2007JA012642

Price, C. P., Swift, D. W., & Lee, L.-C. (1986). Numerical simulation of nonoscillatory mirror waves at the Earth's magnetosheath. *Journal of Geophysical Research*, *91*(A1), 101–112. https://doi.org/10.1029/JA091iA01p00101

Remya, B., Reddy, R. V., Tsurutani, B. T., & Lakhina, G. S. (2017). Comment on "Effects of electron temperature anisotropy on proton mirror instability evolution" by Ahmadi et al. (2016). *Journal of Geophysical Research: Space Physics*, *122*, 745–747. https://doi.org/10.1002/2016JA023148

Remya, B., Reddy, R. V., Tsurutani, B. T., Lakhina, G. S., & Echer, E. (2013). Ion temperature anisotropy instabilities in planetary magnetosheaths. *Journal of Geophysical Research: Space Physics*, *118*, 785–793. https://doi.org/10.1002/jgra50091

Richter, A. K. (1991). Interplanetary slow shocks, space and solar physics. In R. Schwenn & E. Marsch (Eds.), *Physics of the inner heliosphere II* (chap. 7, Vol. 21, pp. 23–44). Berlin: Springer-Verlag.

Richter, I., Auster, H.-U., Berghofer, G., Carr, C., Cupido, E., Fornacon, K.-H., et al. (2016). Two-point observations of low-frequency waves at 67P/Churyumov-Gerasimenko during the descent of PHILAE: Comparison of RPCMAG and ROMAP (2016). *Annales Geophysicae*, *34*(7), 609–622. https://doi.org/10.5194/angeo-34-609-2016

Richter, I., Koenders, C., Auster, H.-U., Frühauff, D., Götz, C., Heinisch, P., et al. (2015). Observation of a new type of low-frequency waves at comet 67P/Churyumov-Gerasimenko. *Annales Geophysice*, *33*(8), 1031–1036. https://doi.org/10.5194/angeo-33-1031-2015

Riley, P., Sonett, C. P., Balogh, A., Forsyth, R. J., Scime, E. E., & Feldman, W. C. (1995). Alfvénic fluctuations in the solar wind: A case study using Ulysses measurements. *Space Science Reviews*, *72*(1-2), 197–200. https://doi.org/10.1007/BF00768779

Riley, P., Sonett, C. P., Tsurutani, B. T., Balogh, A., Forsyth, R. J., & Hoogeveen, G. W. (1996). Properties of arc-polarized Alfvén waves in the ecliptic plane: Ulysses observations. *Journal of Geophysical Research*, *101*(A9), 19,987–19,993. https://doi.org/10.1029/96JA01743

Roberts, D. A., Goldstein, M. L., Klein, L. W., & Matthaeus, W. H. (1987). Origin and evolution of fluctuations in the solar wind: Helios observations and Helios-Voyager comparisons. *Journal of Geophysical Research*, *92*(A11), 12023. https://doi.org/10.1029/JA092iA11p12023

Roberts, D. A., Goldstein, M. L., Klein, L. W., Matthaeus, W. H., & Ghosh, S. (1992). *Journal of Geophysical Research*, *97*(A11), 17,115–17,130. https://doi.org/10.1029/92JA01144

Roytershteyn, V., Karimabadi, H., & Roberts, A. (2015). Generation of magnetic holes in fully kinetic simulations of collisionless turbulence. *Philosophical Transactions of the Royal Society A*, *373*(2041). https://doi.org/10.1098/rsta.2014.0151

Ruderman, M. S. (2010). Freak waves in laboratory and space plasmas. *The European Physical Journal, Special Topics*, *185*(1), 57–66. https://doi.org/10.1140/epjst/e2010-1238-7

Russell, C. T., Mewaldt, R. A., Luhmann, J. G., Mason, G. M., von Rosenvinge, T. T., et al. (2013). The very unusual interplanetary coronal mass ejection of 2012 July 23: A blast wave mediated by solar energetic particles. *The Astrophysical Journal*, *770*, 38.

Saito, S., Nariyuki, Y., & Umeda, T. (2015). Nonlinear damping of a finite amplitude whistler wave due to modified two stream instability. *Physics of Plasmas*, *22*(7), 072105. https://doi.org/10.1063/1.4926523

Sakai, J. I., Yamamura, W., Sato, S., Washimi, H., Tsiklauri, D., & Vekstein, G. (2005). Particle simulation of plasma heating by a large-amplitude Alfvén wave through its transverse modulation in collisionless plasmas. *New Journal of Physics*, *7*, 233. https://doi.org/10.1088/1367-2630/7/1233

Salem, C., Mangeney, A., Bale, S. D., & Veltri, P. (2009). Solar wind magnetohydrodynamics turbulence: Anomalous scaling and role of intermittency. *Astrophysical Journal*, *702*, 537–553. https://doi.org/10.1088/0004-637X/702/

Sckopke, N. (1966). A general relation between the energy of trapped particles and the disturbance field near the Earth. *Journal of Geophysical Research*, *71*(13), 3125–3130. https://doi.org/10.1029/JZ071i013p03125

Shebalin, J. V., Matthaeus, W. H., & Montgomery, D. (1983). Anisotropy in MHD turbulence due to a mean magnetic field. *Journal of Plasma Physics*, *29*(03), 525–547. https://doi.org/10.1017/S0022377800000933

Smith, E. J. (1973a). Observed properties of interplanetary tangential and rotational discontinuities. *Journal of Geophysical Research*, *78*(13), 2088–2093. https://doi.org/10.1029/JA078i013p02088

Smith, E. J. (1973b). Identification of interplanetary tangential and rotational discontinuities. *Journal of Geophysical Research*, *78*(13), 2054–2063. https://doi.org/10.1029/JA078i013p02054

Smith, E. J., & Tsurutani, B. T. (1976). Magnetosheath Lion Roars. *Journal of Geophysical Research*, *81*, 2261–2266.

Smith, E. J., & Wolfe, J. H. (1976). Observations of interaction regions and corotating shocks between one and five AU: Pioneers 10 and 11. *Geophysical Research Letters*, *3*(3), 137–140. https://doi.org/10.1029/GL003i003p00137

Sonett, C. P., & Abrams, I. J. (1963). The distant geomagnetic field, 3. Disorder and shocks in the magnetopause. *Journal of Geophysical Research*, *68*, 1233.

Sonnerup, B. U., & Cahill, L. J. Jr. (1967). Magnetopause structure and attitude from Explorer 12 observations. *Journal of Geophysical Research*, *72*(1), 171. https://doi.org/10.1029/JZ072i001p00171

Stevens, M. L., & Kasper, J. C. (2007). A scale-free analysis of magnetic holes at 1 AU. *Journal of Geophysical Research*, *112*, A05109. https://doi.org/10.1029/2006JA012116

Subedi, P., Sonsrettee, W., Blasi, P., Ruffolo, D., Matthaeus, W. H., Montgomery, D., et al. (2017). Charged particle diffusion in isotropic random magnetic fields. *The Astrophysical Journal*, *837*(2), 140. https://doi.org/10.3847/1538-4357/aa603a

Suess, S. T., & Nerney, S. F. (2002). Stagnation flow in streamer boundaries. *The Astrophysical Journal*, *565*(2), 1275–1288. https://doi.org/10.1086/324697

Summers, D., Thorne, R. M., & Xiao, F. (1998). Relativistic theory of wave-particle resonant diffusion with application to electron acceleration in the magnetosphere. *Journal of Geophysical Research*, *103*(A9), 20,487–20,500. https://doi.org/10.1029/98JA01740

Sun, P., Jokipii, J. R., & Giacolone, J. (2016). Pitch-angle scattering of energetic charged particles in nearly constant magnitude magnetic turbulence. *The Astrophysical Journal*, *827*(1), 16. https://doi.org/10.3847/0004-637X/827/1/16

Thorne, R. M., & Tsurutani, B. T. (1987). *Resonant interactions between cometary ions and low frequency electromagnetic waves*. Planet. Spa. Sci.

Travnicek, P., Hellinger, P., Taylor, M. G. T., Escoubet, C. P., Dandouras, I., & Lucek, E. (2007). Magnetosheath plasma expansion: Hybrid simulations. *Geophysical Research Letters*, *34*, L15104. https://doi.org/10.1029/2007GL029728

Tsubouchi, K. (2009). Alfvén wave evolution within corotating interaction regions associated with the formation of magnetic holes/decreases. *Journal of Geophysical Research*, *114*, A02101. https://doi.org/10.1029/2008JA0113568

Tsubouchi, K., & Matsumoto, H. (2005). Effect of upstream rotational field on the formation of magnetic depressions in a quasi-perpendicular shock downstream. *Journal of Geophysical Research*, *110*, A04101. https://doi.org/10.1029/2004JA010818

Tsurutani, B. T. (1991). Cometary plasma waves and instabilities. In R. Newburn, J. Rahe, & M. Neugebauer (Eds.), *Comets in the post Halley era* (Vol. 2, pp. 491–502). Noordwijk, Holland: ESA Publications.

Tsurutani, B. T., Brinca, A. L., Buti, B., Smith, E. J., Thorne, R. M., & Matsumoto, H. (1989). Magnetic pulses with durations near the local proton cyclotron period: Comet Giacobini-Zinner. *Journal of Geophysical Research*, *94*(A1), 29. https://doi.org/10.1029/JA094iA01p00029

Tsurutani, B. T., Dasgupta, B., Arballo, J. K., Lakhina, G. S., & Pickett, J. S. (2003). Magnetic field turbulence, electron heating, magnetic holes, proton cyclotron waves and the onset of bipolar pulse (electron hole) events: A possible unifying scenario. *Nonlinear Processes in Geophysics*, *10*(1/2), 27–35. https://doi.org/10.5194/npg-10-27-2003

Tsurutani, B. T., Dasgupta, B., Galvan, C., Neugebauer, M., Lakhina, G. S., Arballo, J. K., et al. (2002). Phase-steepened Alfvén waves, proton perpendicular energization and creation of magnetic holes and magnetic decreases: The ponderomotive force. *Geophysical Research Letters*, *29*(24), 2233. https://doi.org/10.1029/2002 GL015652

Tsurutani, B. T., Echer, E., & Gonzalez, W. D. (2011). The solar and interplanetary causes of the recent minimum in geomagnetic activity (MGA23): A combination of midlatitude small coronal holes, low IMF Bz variances, low solar wind speeds and low solar magnetic fields. *Annales Geophysicae*, *29*(5), 839–849. https://doi.org/10.5194/angeo-29-839-2011

Tsurutani, B. T., Echer, E., Guarnieri, F. L., & Kozyra, J. U. (2008). CAWSES November 7–8, 2004 superstorm: Complex solar and interplanetary features in the post-maximum phase. *Geophysical Research Letters*, *35*, L06S05. https://doi.org/10.1029/2007GL031473

Tsurutani, B. T., Falkowski, B. J., Goetz, C., Henri, P., Vallieres, X., Hajra, R., et al. (2016). Wave properties at the diamagnetic cavity boundary of comet 67P/C.-G., abstract, presented at the Rosetta Workshop, 11 December, 2016, San Francisco, CA.

Tsurutani, B. T., Galvan, C., Arballo, J. K., Winterhalter, D., Sakurai, R., Smith, E. J., et al. (2002). Relationship between discontinuities, magnetic holes, magnetic decreases, and nonlinear Alfvén waves: Ulysses observations over the solar poles. *Geophysical Research Letters*, *29*(11), 1528. https://doi.org/10.1029/2001GL013623

Tsurutani, B. T., Glassmeier, K.-H., & Neubauer, F. M. (1995). An intercomparison of plasma turbulence at three comets: Grigg-Skjellerup, Giacobini-Zinner, and Halley. *Geophysical Research Letters*, *22*(9), 1149–1152. https://doi.org/10.1029/95GL00806

Tsurutani, B. T., Glassmeier, K.-H., & Neugebauer, F. M. (1997). A review of nonlinear low frequency (LF) waves observations in space plasmas: On the development of plasma turbulence. In T. Hada & H. Matsumoto (Eds.), *Nonlinear waves and chaos in space plasmas* (chap. 1, pp. 1–44) Tokyo: Terra Science Publication.

Tsurutani, B. T., & Gonzalez, W. D. (1987). The cause of High-Intensity Long-Duration Continuous AE Activity (HILDCAAs): Interplanetary Alfvén wave trains. *Planetary and Space Science*, *35*(4), 405–412. https://doi.org/10.1016/0032-0633(87)90097-3

Tsurutani, B. T., & Gonzalez, W. D. (1994). The causes of geomagnetic storms during solar maximum. *Eos*, *75*(5), 49–56. https://doi.org/10.1029/94EO00468

Tsurutani, B. T., Gonzalez, W. D., Guarnieri, F., Kamide, Y., Zhou, X., & Arballo, J. K. (2004). Are high-intensity long-duration continuous AE activity (HILDCAA) events substorm expansion events? *Journal of Atmospheric and Solar-Terrestrial Physics*, *66*, 167.

Tsurutani, B. T., Gonzalez, W. D., Gonzalez, A. L. C., Guarnieri, F. L., Gopalswamy, N., Grande, M., et al. (2006). Corotating solar wind streams and recurrent geomagnetic activity: A review. *Journal of Geophysical Research*, *111*, A07S01. https://doi.org/10.1029/2005JA011273

Tsurutani, B. T., Gonzalez, W. D., Gonzalez, A. L. C., Tang, F., Arballo, J. K., & Okada, M. (1995). Interplanetary origin of geomagnetic activity in the declining phase of the solar cycle. *Journal of Geophysical Research*, *100*(A11), 21,717–21,733. https://doi.org/10.1029/95JA01476

Tsurutani, B. T., Gonzalez, W. D., Tang, F., Akasofu, S. I., & Smith, E. J. (1988). Origin of interplanetary southward magnetic fields responsible for major magnetic storms near solar maximum (1978-1979). *Journal of Geophysical Research*, *93*(A8), 8519–8531. https://doi.org/10.1029/JA093iA08p08519

Tsurutani, B. T., Guarnieri, F. L., Echer, E., Lakhina, G. S., & Verkhoglyadova, O. P. (2009). Magnetic decrease formation from $<$1 AU to ~5 AU: Corotating interaction region reverse shocks. *Journal of Geophysical Research*, *114*, A08105. https://doi.org/10.1029/2009JA013927

Tsurutani, B. T., Guarnieri, F. L., Lakhina, G. S., & Hada, T. (2005). Rapid evolution of magnetic decreases (MDs) and discontinuities in the solar wind: ACE and Cluster. *Geophysical Research Letters*, *32*, L10103. https://doi.org/10.1029/2004GL022151

Tsurutani, B. T., & Ho, C. M. (1999). A review of discontinuities and Alfvén waves in interplanetary space: Ulysses results. *Reviews of Geophysics*, *37*(4), 517–541. https://doi.org/10.1029/1999RG900010

Tsurutani, B. T., Ho, C. M., Arballo, J. K., Lakhina, G. S., Glassmeier, K.-H., & Neubauer, F. M. (1997). Nonlinear electromagnetic waves and spherical arc-polarized waves in space plasmas. *Plasma Physics and Controlled Fusion*, *39*(5A), A237–A250. https://doi.org/10.1088/0741-3335/39/5A/022

Tsurutani, B. T., Ho, C. M., Arballo, J. K., Smith, E. J., Goldstein, B. E., Neugebauer, M., et al. (1996). Interplanetary discontinuities and Alfvén waves at high heliographic latitudes: Ulysses. *Journal of Geophysical Research*, *101*(A5), 11,027–11,038. https://doi.org/10.1029/95JA03479

Tsurutani, B. T., Ho, C. M., Smith, E. J., Neugebauer, M., Goldstein, B. E., Mok, J. S., et al. (1994). The relationship between interplanetary discontinuities and Alfvén waves: Ulysses observations. *Geophysical Research Letters*, *21*(21), 2267–2270. https://doi.org/10.1029/94GL02194

Tsurutani, B. T., Horne, R. B., Pickett, J. S., Santolik, O., Schriver, D., & Verkhoglyadova, O. P. (2010). Introduction to the special section on chorus: Chorus and its role in space weather. *Journal of Geophysical Research*, *115*, A00F01. https://doi.org/10.1029/2010JA015870

Tsurutani, B. T., & Lakhina, G. S. (1997). Some basic concepts of wave-particle interactions in collisionless plasmas. *Reviews of Geophysics*, *35*(4), 491–501. https://doi.org/10.1029/97RG02200

Tsurutani, B. T., & Lakhina, G. S. (2004). Cross-field particle diffusion in a collisionless plasma: A nonresonant and resonant mechanism. In *CP703, Plasmas in the laboratory and in the universe* (pp. 123–132). New York: AIP.

Tsurutani, B. T., Lakhina, G. S., Pickett, J. S., Guarnieri, F. L., Lin, N., & Goldstein, B. E. (2005). Nonlinear Alfvén waves, discontinuities, proton perpendicular acceleration, and magnetic holes/decreases in interplanetary space and the magnetosphere: Intermediate shocks? *Nonlinear Processes in Geophysics*, *12*(3), 321–336. https://doi.org/10.5194/npg-12-321-2005

Tsurutani, B. T., Lakhina, G. S., Verkhoglyadova, O. P., Echer, E., & Guarnieri, F. L. (2007). Comment on "Comment on the abundances of rotational and tangential discontinuities in the solar wind" by M. Neugebauer. *Journal of Geophysical Research*, *112*, A03101. https://doi.org/10.1029/2006JA011973

Tsurutani, B. T., Lakhina, G. S., Verkhoglyadova, O. P., Echer, E., Guarnieri, F. L., Narita, Y., & Constantinescu, D. O. (2011). Magnetosheath and heliosheath mirror mode structures, interplanetary magnetic decreases and linear magnetic decreases: Differences and distinguishing features. *Journal of Geophysical Research*, *116*, A02103. https://doi.org/10.1029/2010JA015913

Tsurutani, B. T., Lakhina, G. S., Verkhoglyadova, O. P., Gonzalez, W. D., Echer, E., & Guarnieri, F. L. (2011). A review of interplanetary discontinuities and their geomagnetic effects. *Journal of Atmospheric and Solar - Terrestrial Physics*, *73*(1), 5–19. https://doi.org/10.1016/j.jastp.2010.04.001

Tsurutani, B. T., Lakhina, G. S., Winterhalter, D., Arballo, J. K., Galvan, C., & Sakurai, R. (1999). Energetic particle cross-field diffusion: Interaction with magnetic decreases (MDs). *Nonlinear Processes in Geophysics*, *6*(3/4), 235–242. https://doi.org/10.5194/npg-6-235-1999

Tsurutani, B. T., & Lin, R. P. (1985). Acceleration of $>$47 keV ions and $>$2 keV electrons by interplanetary shocks at 1 AU. *Journal of Geophysical Research*, *90*(A1), 1–11. https://doi.org/10.1029/JA090iA01p00001

Tsurutani, B. T., Page, D. E., Smith, E. J., Goldstein, B. E., Brinca, A. L., Thorne, R. M., et al. (1989). Low Frequency Plasma Waves and Ion Pitch Angle Scattering at Large Distance ($>$350,000 km) from Giacobini-Zinner: IMF a Dependences. *Journal of Geophysical Research*, *94*, 18.

Tsurutani, B. T., & Smith, E. J. (1977). Two types of magnetospheric ELF chorus and their substorm dependences. *Journal of Geophysical Research*, *82*(32), 5112–5128. https://doi.org/10.1029/JA082i032p05112

Tsurutani, B. T., & Smith, E. J. (1979). Interplanetary discontinuities: Temporal variations and the radial gradient from 1 to 8.5 AU. *Journal of Geophysical Research*, *84*, 2773.

Tsurutani, B. T., & Smith, E. J. (1986a). Strong hydromagnetic turbulence associated with comet Giacobini-Zinner. *Geophysical Research Letters*, *13*(3), 259–262. https://doi.org/10.1029/GL013i003p00259

Tsurutani, B. T., & Smith, E. J. (1986b). Hydromagnetic waves and instabilities associated with cometary ion pickup: ICE observations. *Geophysical Research Letters*, *13*(3), 263–266. https://doi.org/10.1029/GL013i003p00263

Tsurutani, B. T., Smith, E. J., Anderson, R. R., Ogilvie, K. W., Scudder, J. D., Baker, D. N., & Bame, S. J. (1982). Lion roars and nonoscillatory drift mirror waves in the magnetosheath. *Journal of Geophysical Research*, *87*(A8), 6060–6072. https://doi.org/10.1029/JA087iA08p06060

Tsurutani, B. T., Smith, E. J., Ho, C. M., Neugebauer, M., Goldtein, B. E., Mok, J. S., et al. (1995). Interplanetary discontinuities and Alfvén waves. *Space Science Reviews*, *72*(1-2), 205–210. https://doi.org/10.1007/BF00768781

Tsurutani, B. T., Smith, E. J., Pyle, K. R., & Simpson, J. A. (1982). Energetic protons accelerated at corotating shocks: Pioneer 10 and 11 observations from 1 to 6 AU. *Journal of Geophysical Research*, *87*(A9), 7389–7404. https://doi.org/10.1029/JA087iA09p07389

Tsurutani, B. T., Smith, E. J., West, H. I. Jr., & Buck, R. M. (1979). Chorus, energetic electrons and magnetospheric substorms. In P. J. Palmadesso & K. Papadopoulos (Eds.), *Instabilities in space plasmas* ( pp. 55–62). Dordrecht, Netherlands: D. Reidel.

Tsurutani, B. T., Thorne, R. M., Smith, E. J., Gosling, J. T., & Matsumoto, H. (1987). Steepened magnetosonic waves at comet Giacobini-Zinner. *Journal of Geophysical Research*, *92*(A10), 11,074–11,082. https://doi.org/10.1029/JA092iA10p11074

Turner, D. L., & Li, X. (2008). Quantitative forecast of relativistic electron flux at geosynchronous orbit based on low-energy electron flux. *Space Weather*, *6*, S05005. https://doi.org/10.1029/2007SW000354

Turner, J. M., Burlaga, L. F., Ness, N. F., & Lemaire, J. F. (1977). Magnetic holes in the solar wind. *Journal of Geophysical Research*, *82*(13), 1921–1924. https://doi.org/10.1029/JA082i013p01921

Turner, N. E., Mitchell, E. J., Knipp, D. J., & Emery, B. A. (2006). Energetics of magnetic storms driven by corotating interplanetary regions: A study of geoeffectiveness. In B. T. Tsurutani, R. McPherron, W. Gonzalez, et al. (Eds.), *Recurrent magnetic storms: Corotating solar wind streams* (Vol. 167, pp. 113–124). Washington, DC: AGU Press.

Vasquez, B. J., Abramenko, V. I., Haggerty, D. K., & Smith, C. W. (2007). Numerous small magnetic discontinuities of Bartels rotation 2286 and the potential role of Alfvénic turbulence. *Journal of Geophysical Research*, *112*, A11102. https://doi.org/10.1029/2007JA012504

Vasquez, B. J., & Hollweg, J. V. (1999). Formation of pressure balance structures and fast waves from nonlinear Alfvén waves. *Journal of Geophysical Research*, *104*(A3), 4681–4696. https://doi.org/10.1029/1998JA900090

Verdini, A., & Grappin, R. (2016). Beyond the Maltese cross: Geometry of turbulence between 0.2 and 1 au. *The Astrophysical Journal*, *831*(179). https://doi.org/10.3847/0004-637X/831/2/179

Verma, M. K. (2004). Statistical theory of magnetohydrodynamic turbulence: Recent results. *Physics Reports*, *401*(5-6), 229–380. https://doi.org/10.1016/j.physrep.2004.07.007

Volwerk, M., Schmid, D., Tsurutani, B. T., Delva, M., Plaschke, F., Narita, Y., et al. (2016). Mirror mode waves in Venus's magnetosheath: Solar minimum vs. solar maximum. *Annales Geophysicae*, *34*(11), 1099–1108. https://doi.org/10.5194/angeo-34-1099-2016

Volwerk, M., Zhang, T. L., Delva, M., Voros, Z., Baumjohann, W., & Glassmeier, K.-H. (2008). First identification of mirror mode waves in Venus' magnetosheath? *Geophysical Research Letters*, *35*, L12204. https://doi.org/10.1029/2008GL033621

Winterhalter, D., Neugebauer, M., Goldstein, B. E., Smith, E. J., Bame, S. J., & Balogh, A. (1994). Ulysses field and plasma observations of magnetic holes in the solar wind and their relation to mirror-mode structures. *Journal of Geophysical Research*, *99*(A12), 23,371–23,381. https://doi.org/10.1029/94JA01977

Winterhalter, D., Neugebauer, M., Goldstein, B. E., Smith, E. J., Tsurutani, B. T., Bame, S. J., & Balogh, A. (1995). Magnetic holes in the solar wind and their relation to mirror-mode structures. *Space Science Reviews*, *72*(1-2), 201–204. https://doi.org/10.1007/BF00768780

Winterhalter, D., Smith, E. J., Neugebauer, M., Goldstein, B. E., & Tsurutani, B. T. (2000). The latitudinal distribution of solar wind magnetic holes. *Geophysical Research Letters*, *27*(11), 1615–1618. https://doi.org/10.1029/1999GL003717

Wu, C. C. (1987). On MHD intermediate shocks. *Geophysical Research Letters*, *14*(6), 668–671. https://doi.org/10.1029/GL014i006p00668

Wu, C. S., & Davidson, R. C. (1972). Electromagnetic instabilities produced by neutral-particle ionization in interplanetary space. *Journal of Geophysical Research*, *77*(28), 5399–5406. https://doi.org/10.1029/JA077i028p05399